

1       **Spring tropical cyclones modulate near-surface isotopic compositions of**  
2                                   **atmospheric water vapour at Kathmandu, Nepal**

3       Niranjan Adhikari<sup>1,2</sup>, Jing Gao<sup>1,3\*</sup>, Aibin Zhao<sup>1</sup>, Tianli Xu<sup>1,4</sup> Manli Chen<sup>1,3</sup>,  
4                                   Xiaowei Niu<sup>1</sup>, Tandong Yao<sup>1,3</sup>

5       <sup>1</sup> *State Key Laboratory of Tibetan Plateau Earth System, Resources and Environment, Institute*  
6       *of Tibetan Plateau Research, Chinese Academy of Sciences, Beijing 100101, China*

7       <sup>2</sup> *University of Chinese Academy of Sciences, Beijing 100049, China*

8       <sup>3</sup> *Lanzhou University, Lanzhou 733000, China*

9       <sup>4</sup> *Kathmandu Centre for Research and Education, Chinese Academy of Sciences –Tribhuvan*  
10       *University, Kirtipur 44613, Kathmandu, Nepal*

11       \* Correspondence to: Jing Gao, E-mail: [gaojing@itpcas.ac.cn](mailto:gaojing@itpcas.ac.cn)

12  
13       **Abstract**

14       While westerlies are recognized as a significant moisture transport in Nepal during the pre-  
15       monsoon season, precipitation is also attributed to moisture from cyclones originating in the Bay  
16       of Bengal (BoB) or the Arabian Sea (AS). Tropical cyclones exhibit negative isotopic values in  
17       both precipitation and atmospheric water vapour; however, the factors influencing isotopic  
18       fractionation during tropical cyclones remain poorly understood. We present the results of  
19       continuous measurements of the isotopic composition of atmospheric water vapour ( $\delta^{18}\text{O}_v$ ,  $\delta\text{D}_v$ ,  
20       and d-excess<sub>v</sub>) at Kathmandu from 7 May to 7 June 2021 during two pre-monsoon cyclones;  
21       cyclone Tauktae formed over the Arabian Sea, and cyclone Yaas formed over the Bay of Bengal.  
22       Our study reveals that tropical cyclones originating from the BoB and the AS during the pre-

23 monsoon season modulate isotopic signals of near-surface atmospheric water vapour in Nepal.  
24 Comparing conditions before and after, we observed a significant depletion of  $\delta^{18}\text{O}_v$  and  $\delta\text{D}_v$   
25 during both cyclones, attributed to changes in moisture sources (local vs. marine). Convective  
26 activity plays a pivotal role in the variability of  $\delta^{18}\text{O}_v$  and  $\delta\text{D}_v$  during both cyclones, confirmed  
27 by the spatial variations of outgoing longwave radiation (OLR) and regional precipitation during  
28 both cyclones. We also found a significant negative correlation between  $\delta^{18}\text{O}_v/\delta\text{D}_v$  and rainfall  
29 amount along the trajectories during cyclone Tauktae, probably resulting from integrated  
30 upstream processes linked to the earlier Rayleigh distillation of water vapour via rainfall, rather  
31 than local rainfall. The decrease in  $\delta^{18}\text{O}_v/\delta\text{D}_v$  during cyclone Yaas is associated with the  
32 intensified convection and moisture convergence at the measurement site, while the lower cloud  
33 top temperatures (CTT) and lower cloud top pressure (CTP) during intense convection contribute  
34 to higher d-excess values at the final stage of cyclone Yaas. This characteristic is missing during  
35 cyclone Tauktae. Our results shed light on key processes governing the isotopic composition of  
36 atmospheric water vapour at Kathmandu with implications for the monsoon moisture transport  
37 and paleoclimate reconstructions of tropical cyclone activity.

38 Keywords: Cyclones; Isotopic composition of atmospheric water vapour; Convection; Moisture  
39 convergence; Kathmandu

40

41

42

## 43 **1 Introduction**

44 Although the Indian summer monsoon accounts for more than 80 % of annual rainfall in Nepal,  
45 agricultural activities also rely on precipitation in the pre-monsoon season. Pre-monsoonal  
46 rainfall in Nepal is often associated with cyclonic events that provide precipitation to support the  
47 timely planting of monsoonal crops. Previous studies have suggested that extreme precipitation  
48 in Nepal is mostly fuelled by moisture from the Arabian Sea (AS) and the Bay of Bengal (BoB)  
49 (Bohlinger et al., 2017; Boschi and Lucarini, 2019). Higher sea surface temperatures and the  
50 westward movement of tropical cyclones formed over the Western Pacific result in cyclones  
51 being formed over the BoB and the AS (Mohapatra et al., 2016). The number of cyclones in the  
52 AS has increased recently compared to the number of cyclones in the BoB (Pandya et al., 2021).  
53 According to the International Best Track Archive for Climate Stewardship (IBTrACS) project,  
54 in 2019 three cyclones originated in the BoB and five cyclones originated in the AS, due to a rise  
55 in sea surface temperature lengthening the cyclone decay period (Li and Chakraborty, 2020).  
56 Usually, the impact of cyclones formed over the AS is restricted to the nearest coastal regions.  
57 However, in recent years this appears to have changed as cyclones are forming back-to-back  
58 over the AS and affecting the entire Indian subcontinent including surrounding regions (Li and  
59 Chakraborty, 2020). Cyclone Tauktae affected the livelihoods of people both near the coast and  
60 further inland during the pre-monsoon season of 2021 (Pandya et al., 2021). The impacts of  
61 cyclone Yaas after cyclone Tauktae were also felt in Nepal, where it triggered flooding and  
62 landslides in several parts of the country ([https://floodlist.com/asia/nepal-flood-landslide-may-  
63 2021/](https://floodlist.com/asia/nepal-flood-landslide-may-2021/)). As both cyclones hit in short succession, this led to severe agricultural damage in several  
64 parts of India at a critical time when farmers were preparing to sow their rice paddies ahead of  
65 the monsoon season (<https://reliefweb.int/organization/acaps>). In Nepal, the damage due to Yaas

66 was mostly limited to the Terai regions which experienced intense and continuous rainfall  
67 (<https://kathmandupost.com/>). Moisture flux associated with cyclones generally extends over a  
68 large area and causes moderate to heavy precipitation along the cyclone path and on the nearest  
69 land mass (Chan et al., 2022; Rajeev and Mishra, 2022). It is therefore essential to understand the  
70 moisture transport processes of these extreme rainfall events on atmospheric water vapour.

71 With climate change, the amount of water vapour in the atmosphere is also expected to increase,  
72 creating scientific interest in the impact of atmospheric water vapour on changing moisture  
73 patterns (Hoffmann et al., 2005). The isotopic composition of atmospheric water vapour ( $\delta^{18}\text{O}_v$ ,  
74  $\delta\text{D}_v$ , and  $d\text{-excess}_v$ ) contains comprehensive information about the history of moisture exchange  
75 (Noone, 2012; Payne et al., 2007; Risi et al., 2008; Worden et al., 2007). Several studies have  
76 shown that isotopic composition is an effective indicator of cyclone activity (Munksgaard et al.,  
77 2015; Sun et al., 2022) including cyclone evolution and structure (Lawrence et al., 2002). The  
78 atmospheric water vapour and precipitation associated with tropical cyclones tend to have  
79 extremely depleted isotopic compositions compared to monsoonal rain (Chen et al., 2021;  
80 Jackisch et al., 2022; Munksgaard et al., 2015; Sánchez-Murillo et al., 2019), which may be due  
81 to the high condensation efficiency and substantial fractionation associated with cyclones. A few  
82 studies found a systematic depletion of heavy isotopes towards the cyclone eye (Lawrence et al.,  
83 2002, 1998; Lawrence and Gedzelman, 1996; Sun et al., 2022; Xu et al., 2019). For example,  
84 during cyclone Shanshan, Fudeyasu (2008) observed that isotopic depletion in precipitation and  
85 water vapour increased radially inward in the cyclone's outer region, likely due to a rainout  
86 effect. A study conducted in north-eastern Australia during cyclone Ita in April 2014 underlined  
87 the role of synoptic-scale meteorological settings in determining the isotopic variability of  
88 atmospheric water vapour (Munksgaard et al., 2015). In Fuzhou, China, Xu et al., (2019)

89 reported a significant depletion in typhoon rain  $\delta^{18}\text{O}$  related to the combined effect of large-scale  
90 convection, high condensation efficiency, and recycling of isotopically depleted vapour in the  
91 rain shield area. Sánchez-Murillo et al., (2019) highlighted the role of convective and stratiform  
92 activity as well as precipitation type and amount. The impact of high stratiform fractions and  
93 deep convection on isotopic depletion in precipitation during typhoon Lekima was confirmed by  
94 Han et al., (2021).

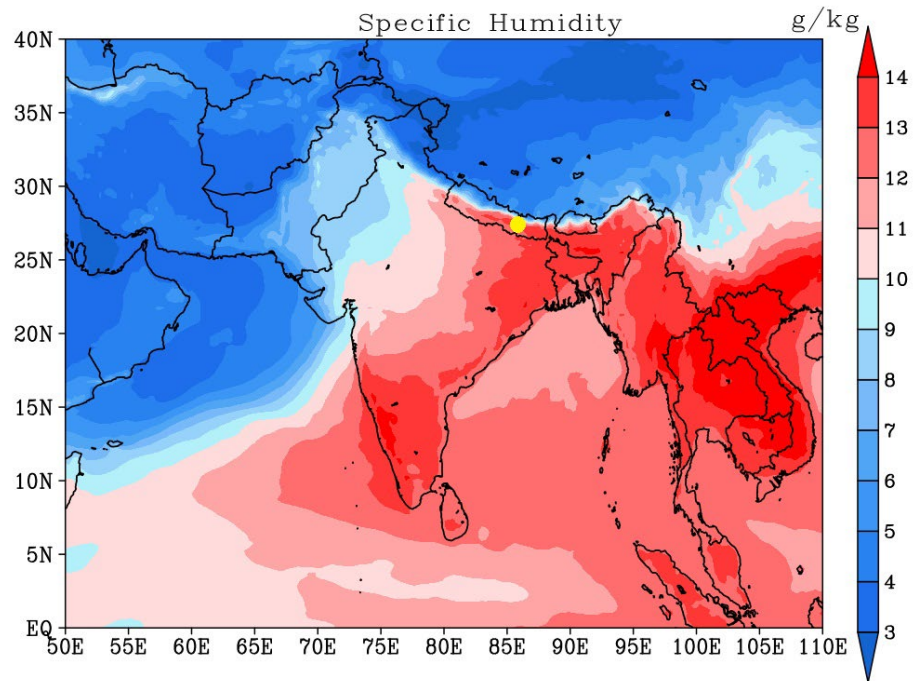
95 Although several studies have examined the isotopic variation of event-based precipitation in  
96 Nepal (Acharya et al., 2020; Adhikari et al., 2020; Chhetri et al., 2014), there remains a  
97 knowledge gap regarding the isotopic response of atmospheric water vapour during cyclone  
98 events. We present for the first time the evolution of the isotopic composition of atmospheric  
99 water vapour ( $\delta^{18}\text{O}_v$ ,  $\delta\text{D}_v$ , and d-excess) in Kathmandu including two pre-monsoon cyclone  
100 events. Isotopic data were collected in 2021, from one week before to one week after the  
101 cyclones. Although neither cyclone passed directly over Kathmandu, their remnant vapour  
102 produced several days of rainfall that allowed us to observe changes in the isotopic composition  
103 at high temporal resolution and evaluate the cause of such changes at diurnal scales.

## 104 **2 Data and methods**

### 105 **2.1 Site description**

106 The Kathmandu station lies on the southern slope of the Himalayas (27°42' N, 85°20' E) at an  
107 altitude of approximately 1400 m above sea level. Based on an 18-year-long record from the  
108 Department of Hydrology and Meteorology, Government of Nepal (2001 to 2018), this region  
109 has an average annual temperature of 19° C and precipitation amount of about 1500 mm, with  
110 ~78% of the annual rainfall occurring in the monsoon season from June to September (Adhikari  
111 et al., 2020). About 16 % of annual rainfall in Kathmandu occurs in the pre-monsoon season

112 (March to May) with air temperature ranges from 13 to 28° C and averaged relative humidity  
113 (RH) of 67 %. Advection of the southern branch of westerlies and evaporation from nearby water  
114 bodies are the main contributors to pre-monsoonal precipitation (Yu et al., 2015; Chhetri et al.,  
115 2014). These arid westerlies, resulted in diminished temperature and relative humidity (RH)  
116 within the region while a substantial presence of moisture was observed over extensive areas  
117 encompassing the BoB, the AS, India, and surrounding regions including our sampling site  
118 during our study period. Figure 1 shows the elevated specific humidity levels averaged between  
119 1000 hPa and 850 hPa throughout the duration of our study period.



120  
121 **Figure 1 Spatial distribution of specific humidity averaged over 1000 hPa to 850 hPa (in**  
122 **g/Kg) during the period of study. The yellow dot shows the location of Kathmandu.**

## 123 **2.2 The evolution of cyclones Tauktae and Yaas and weather conditions at** 124 **Kathmandu**

125 Cyclone Tauktae developed as a tropical disturbance on 13 May 2021 over the AS, evolved into  
126 a deep depression by 14 May, moved north, and gradually intensified before turning into a  
127 cyclonic storm with wind speeds reaching 75 km/h on that same day (Pandya et al., 2021). After  
128 making landfall in the Gir-Somnath district of Gujarat, Tauktae continued to strengthen and was  
129 classified as an extremely severe cyclonic storm on 17 May reaching maximum wind speeds of  
130 220 km/h (Verma and Gupta, 2021; Pandya et al., 2021). Tauktae weakened into a low  
131 depression on 18 May 2021 at 17:00 h Indian Local Time (ILT) and finally dissipated one day  
132 later. Due to its large convective area, it brought heavy rainfall to different regions of India and  
133 Nepal.

134 The signal of cyclone Tauktae was first detected at the Kathmandu site on 19 May at  
135 approximately 03:00 local time (LT), followed by light drizzle. The recorded air temperature was  
136 about 22°C, and the relative humidity (RH) was approximately 72%. Within 16 hours, the RH  
137 increased from 72% to 91%, while the temperature dropped from 22°C to around 19°C. The  
138 maximum RH and minimum temperature were observed on 21 May around 04:00 h LT, reaching  
139 92% and 17°C, respectively.

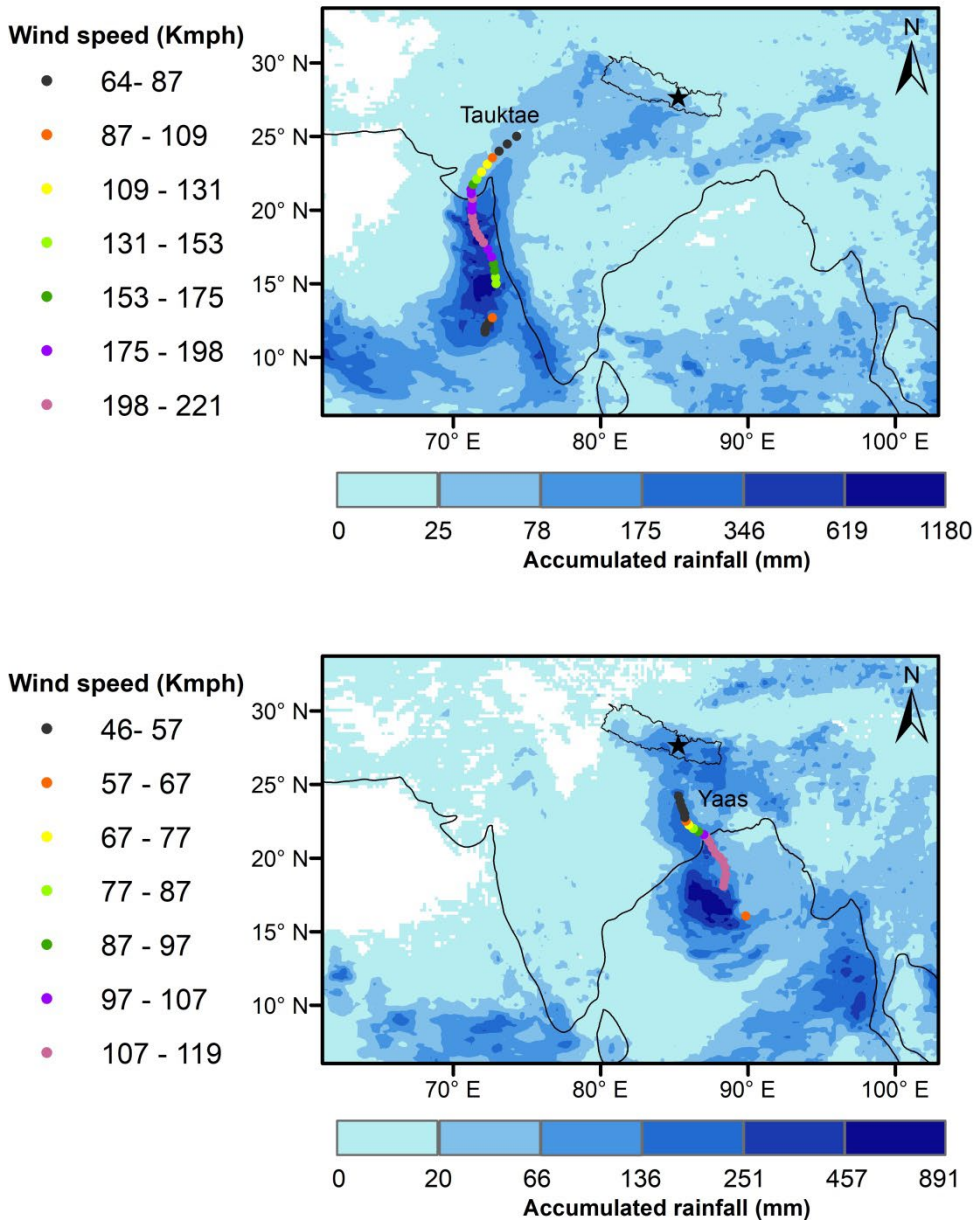
140 Cyclone Yaas started out as a depression over the BoB on 22 May 2021 at 08:30 h ILT and  
141 gradually intensified into a deep depression before turning into a cyclonic storm on 24 May at  
142 00:00 h ILT as it moved northeast (Paul and Chowdhury, 2021). The corresponding wind speed  
143 and central pressure were recorded as 65 km/h and 990 hPa, respectively. On 24 May around  
144 18:00 h ILT, it intensified into a severe cyclonic storm with wind speeds ranging from 89 to 117  
145 km/h before becoming a very severe cyclonic storm on 25 May at 12:00 h ILT with wind speeds

146 from 119 km/h to 165 km/h. It made landfall north of Odisha on 26 May with maximum  
147 sustained wind speeds of 130 km/h to 140 km/h and progressively weakened into a depression on  
148 27 May before dissipating over northern India on 28 May.

149 The Kathmandu weather station recorded a total of 59.6 mm of precipitation during cyclone  
150 Yaas. Intermittent small patches of rainfall commenced on 25 May at 11:00h LT. The main  
151 cyclone event occurred from 26 May at 01:00h LT to 29 May at 01:00h LT. Throughout this  
152 period, the ground-level RH fluctuated between 84% and 93%, while surface temperature varied  
153 between 18°C and 22°C. Notably, all RH values exceeded 80% from 25 May around 22:00 h LT  
154 to 29 May at 10:00 h LT.

155 Wind speeds, pressure, and cyclone eye location information (3-hour resolution) were taken from  
156 datasets of the International Best Track Archive for Climate Stewardship (IBTrACS) project  
157 (Knapp et al., 2010), <https://www.ncei.noaa.gov/products/>. The latter was used to calculate the  
158 spatial distance between the cyclone's eye and our measurement location. Figure 2 illustrates the  
159 intensity and cumulative rainfall along the paths of the cyclones. A characteristic of both  
160 cyclones is the occurrence of rainout along their trajectories, persisting as they move inland.





161

162

**Figure 2 The intensity and track of cyclone Tauktae (Upper panel) and Yaas (Bottom panel)**

163

**along with accumulated rainfall during their occurrence.**

164

### 165 **2.3 Isotope measurements**

166 Near-surface  $\delta^{18}\text{O}_v$  and  $\delta\text{D}_v$  were measured continuously using a Picarro L2130-i analyser based  
167 on wavelength-scanned cavity ring-down spectroscopy (WS-CRDS) (Brand et al., 2009), located  
168 at the Kathmandu Centre for Research and Education (KCRE), Nepal. The sampling inlet  
169 consisting of a heated copper tube mounted 7 m above the ground protected with a plastic hood  
170 and a  $10 \text{ L min}^{-1}$  pump transported the sample from the inlet to the analyser. The automated  
171 standard delivery module (SDM) was used for calibration, with each calibration made using two  
172 reference standards calibrated against Vienna Standard Mean Ocean Water (VSMOW), covering  
173 the isotopic ranges of ambient water vapour at Kathmandu. Each reference standard was  
174 measured continuously for a total of 75 min each day at three different humidity levels (25  
175 minutes per level). The dry air passed through Drierite™ desiccant (Merck, Germany) and was  
176 delivered to the Picarro analyser for standard measurements. The isotopic composition of  
177 atmospheric water vapour is reported as parts per thousand (‰) relative to VSMOW using

$$178 \quad \delta^* = (R_A / R_S - 1) \times 1000 \text{ [‰]}, \quad (1)$$

179 where  $\delta^*$  represents either  $\delta\text{D}_v$  or  $\delta^{18}\text{O}_v$ , and  $R_A$  and  $R_S$  denote the ratios of heavy to light  
180 isotopes ( $^{18}\text{O}/^{16}\text{O}$  or  $\text{D}/\text{H}$ ) in the sample and standard, respectively (Kendall & Caldwell, 1998;  
181 Yoshimura, 2015). As suggested by Dansgaard, (1964), deuterium excess ( $\text{d-excess}_v = \delta\text{D}_v - 8 \times \delta^{18}\text{O}_v$ )  
182 is used as a tracer for moisture source conditions (Liu et al., 2008; Tian et al., 2001). We  
183 examined the hourly isotopic composition of atmospheric water vapour between 7 May and 7  
184 June 2021, covering the Tauktae and Yaas cyclones including one week on either side.  
185

## 186 **2.4 Meteorological data**

187 An automated weather station (AWS, Davis Vantage Pro2) continuously measured air  
188 temperature, relative humidity, dew point temperature, wind speed and direction, rainfall amount,  
189 surface pressure, etc. at one-minute intervals from 7 May to 7 June 2021.

190 We used Integrated Multi-satellite Retrievals for GPM (IMERG) from the Global Precipitation  
191 Measurement (GPM) program with a spatial resolution of  $0.1^\circ$  latitude and longitude (Huffman  
192 et al., 2017) to analyse the regional rainfall intensity before, during, and after the cyclone events.  
193 These high-resolution data allow for the identification of convective rainfall areas and the  
194 passage of tropical cyclones (Jackisch et al., 2022). They have been used previously to depict  
195 cyclone tracks and associated rainfall intensities (Gaona et al., 2018; Jackisch et al., 2022;  
196 Villarini et al., 2011).

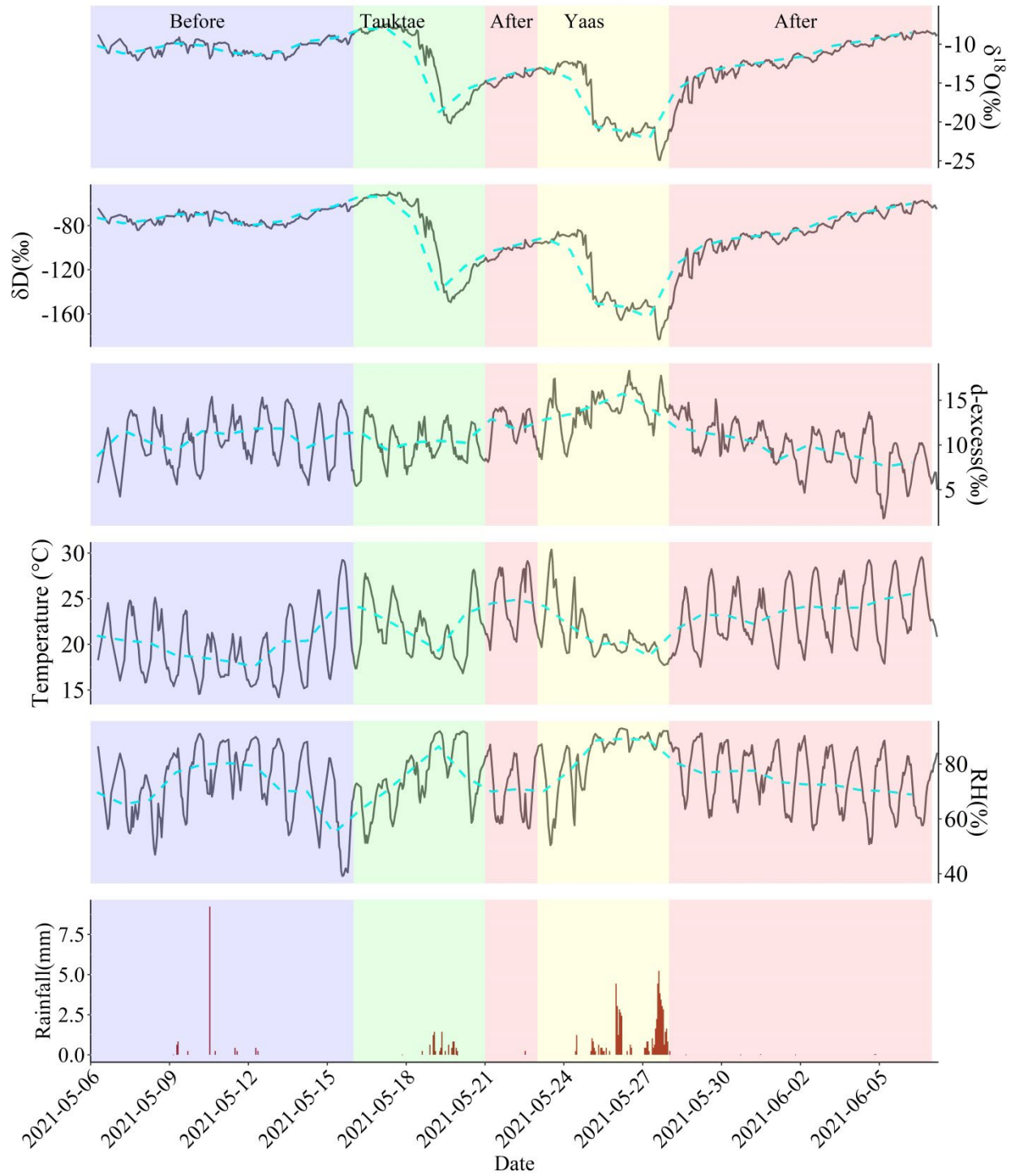
197 We further obtained outgoing longwave radiation (OLR), zonal and meridional wind, specific  
198 humidity, vertical velocity, pressure, and distribution of relative humidity and temperature data  
199 from ERA5 datasets (Herbath et al., 2020) with a spatial resolution of  $0.25^\circ$  from longitude-  
200 latitude grids (<https://cds.climate.copernicus.eu/>). OLR data has already been used as an index of  
201 tropical convection (Liebmann and Smith, 1996). Additionally, we used cloud-top pressure (CTP)  
202 and cloud-top temperature (CTT) data from MERRA-2 Reanalysis datasets retrieved from  
203 <https://giovanni.gsfc.nasa.gov/>, with a spatial resolution of  $0.5^\circ \times 0.625^\circ$ , as indicators of  
204 convective intensity.

## 205 **2.5 Moisture backward trajectory analysis**

206 To assess the influence of moisture transport history on the isotopic composition of atmospheric  
207 water vapour before, during, and after the cyclone events, we analysed five-day moisture  
208 backward trajectories that terminated at the sampling site using the Hybrid Single-Particle

209 Lagrangian Integrated Trajectory (HYSPLIT) model (Draxler and Hess, 1997). The Global Data  
210 Assimilation System (GDAS) with a spatial resolution of  $1^\circ$  (Kleist et al., 2009) was used to  
211 provide the meteorological forcing for the HYSPLIT model. Variations in specific humidity  
212 along the moisture trajectories were also calculated. Considering the variation in boundary layer  
213 height at Kathmandu during the study period, ranging from approximately 100 m to 1170 m, and  
214 with the majority of the data falling below 600 m, we set the initial starting height for the  
215 moisture backward trajectories to 500 m above ground.

216 **3 Results**



217

218 **Figure 3 Water vapour isotopic evolution (hourly averages) before, during, and after the**  
219 **Tauktae and Yaas cyclone events along with associated surface air temperature, relative**  
220 **humidity (RH), and rainfall amount. The cyan dashed line represents daily variations.**

221 Significant variability was observed in isotopic composition before, during, and after the  
222 cyclones at Kathmandu station (Fig. 3 and Table 1).  $\delta^{18}\text{O}_v$  and  $\delta\text{D}_v$  showed a sudden depletion in  
223 the final stages of both cyclones, coinciding with RH reaching maximum values. The depletion  
224 was more pronounced during cyclone Yaas compared to cyclone Tauktae.

225 Before the cyclone Tauktae,  $\delta^{18}\text{O}_v$  ( $\delta\text{D}_v$ ) varied from -7.40 ‰ (-49.53 ‰) to -12.10 ‰ (-84.15 ‰)  
226 with an average of -10.04 ‰ (-69.51 ‰) and  $d\text{-excess}_v$  ranged from 4.24 ‰ to 15.38 ‰ with an  
227 average of 10.84 ‰. The isotopic composition clearly shows a downward trend as the remnant of  
228 cyclones passed over Kathmandu.  $\delta^{18}\text{O}_v$  decreased by over 12 ‰ from 14 May to 20 May  
229 (Tauktae) and again between 24 May and 29 May (Yaas), reaching minima for  $\delta^{18}\text{O}_v$  ( $\delta\text{D}_v$ ) of -  
230 20.21 ‰ (-149.49 ‰) and -24.92 ‰ (-183.34 ‰), respectively. During Tauktae,  $\delta^{18}\text{O}_v$  ( $\delta\text{D}_v$ )  
231 varied from -8.20‰ (-56.06‰) to -20.21‰ (-149.49‰) with an average of -14.73‰ (-106.76‰)  
232 and during Yaas  $\delta^{18}\text{O}_v$  ( $\delta\text{D}_v$ ) ranges from -12.17‰ (-83.85‰) to -24.92‰ (-183.34‰) with an  
233 average of -17.87‰ (-129.18‰). Similarly,  $d\text{-excess}_v$  during Tauktae varied from 7.97 ‰ to  
234 14.24 ‰ with an average of 11.06 ‰ while during Yaas it varied from 8.71 ‰ to 18.29 ‰ with  
235 an average of 13.77 ‰. After both cyclones had dissipated,  $\delta^{18}\text{O}_v$  (and  $\delta\text{D}_v$ ) started to recover  
236 pre-cyclone values of -8.29 ‰ to -14.94 ‰ (-57.40 ‰ to -109.31 ‰), with an average of -11.09 ‰  
237 (-79.38 ‰), and  $d\text{-excess}$  ranged between 1.80 ‰ and 15.11 ‰ with an average of 9.37 ‰.

238 The remnants of cyclone Tauktae caused light rain at Kathmandu, with a significant depletion in  
239  $\delta^{18}\text{O}_v$  ( $\delta\text{D}_v$ ) by ~8 ‰ (~66 ‰) on 20 May compared to the previous day. From the formation of a

240 depression over the AS on 14 May 2021 until the dissipation inland on 19 May (Fig. S3), no  
241 significant variation in the isotopic composition in atmospheric water vapour at Kathmandu was  
242 observed (Fig. 3). After the dissipation, when the residual Tauktae vapour passed the Kathmandu  
243 site producing light rains,  $\delta^{18}\text{O}_v$  and  $\delta\text{D}_v$  began to decrease independently of the rainfall amount,  
244 starting on 19 May around 11:00 h Local Time (LT), from -8.34 ‰ for  $\delta^{18}\text{O}_v$  and -56.06 ‰ for  
245  $\delta\text{D}_v$  and decreasing in one hour to -10.12 ‰ and -68.41 ‰ respectively. This decrease continued  
246 for 24 hours reaching a minimum of -20.21 ‰ and -149.49 ‰ for  $\delta^{18}\text{O}_v$  and  $\delta\text{D}_v$  respectively on  
247 20 May at 12:00 h LT. However,  $d\text{-excess}_v$  did not show notable variations during the passage of  
248 cyclone Tauktae.  $\delta^{18}\text{O}_v$  and  $\delta\text{D}_v$  remained depleted from 20 to 22 May.

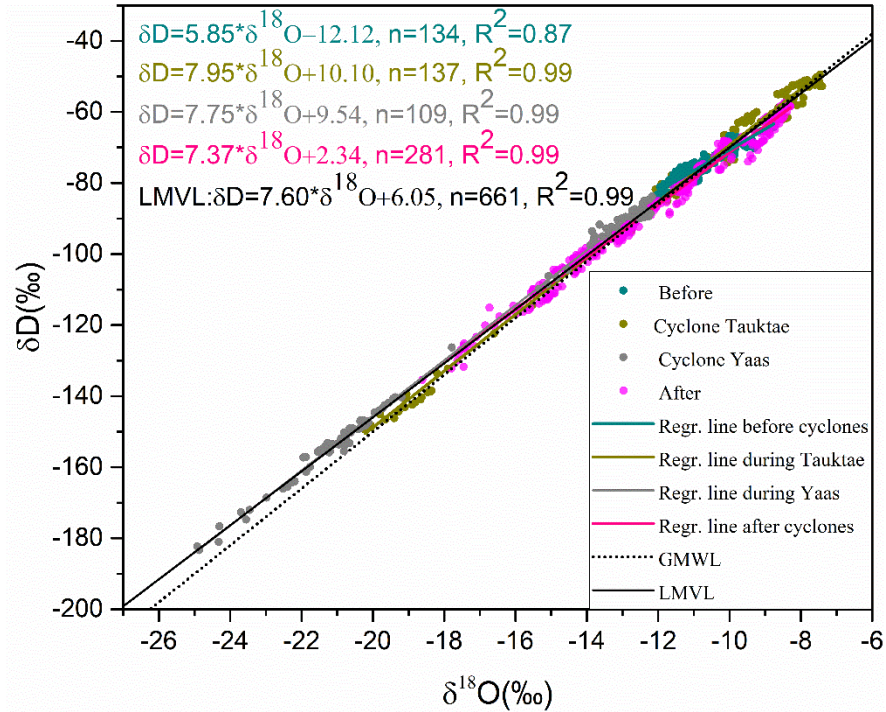
249 On 24 May, cyclone Yaas formed over the BoB and followed a trajectory through north-eastern  
250 India (Fig. S4). The effect of cyclone Yaas on  $\delta^{18}\text{O}_v$  and  $\delta\text{D}_v$  at Kathmandu was observed on 25  
251 May with  $\delta^{18}\text{O}_v$  ( $\delta\text{D}_v$ ) dropping rapidly from -12.62 ‰ (-88.71 ‰) on 25 May at 20:00 h LT to -  
252 15.07 ‰ (-106.22 ‰) just one hour later. At the same time,  $d\text{-excess}_v$  increased from 12.30 ‰ to  
253 14.34 ‰. The depletion continued until 28 May with a minimum of  $\delta^{18}\text{O}_v$  ( $\delta\text{D}_v$ ) by -24.92 ‰ (-  
254 182.35 ‰) at 16:00 h LT. Yaas had already weakened into a low-pressure area over Bihar in  
255 south-eastern Uttar Pradesh, India.  $\delta^{18}\text{O}_v$  and  $\delta\text{D}_v$  started to increase by about 10 ‰ on 29 May  
256 at 16:00 h LT after Yaas had dissipated. From 25 to 29 May,  $d\text{-excess}_v$  gradually increased as  
257 opposed to  $\delta^{18}\text{O}_v$  and  $\delta\text{D}_v$ , resulting in a negative correlation with  $\delta^{18}\text{O}_v$  and  $\delta\text{D}_v$  of -0.60 and -  
258 0.55 respectively.

259 The passage of cyclones that had formed over the AS (Tauktae) and BoB (Yaas) caused  
260 significant depletion in the isotopic composition and led to cumulative rainfall of 9.2 mm  
261 (Tauktae) between 14 May and 20 May 2021 and 59.6 mm (Yaas) between 25 May and 28 May  
262 2021 at our site. This depletion is due to cyclone-associated intense rainfall and agrees with

263 previous studies (Krishnamurthy and Shukla, 2007; Rahul et al., 2016). Note the above  $\delta^{18}\text{O}_v$   
264 minimum (-24.92 ‰) observed during cyclone Yaas is similar to the minima observed in  
265 Bangalore, India ( $\delta^{18}\text{O}_v = -22.5$  ‰) (Rahul et al., 2016) and Roorkee, India ( $\delta^{18}\text{O}_v = -25.35$  ‰)  
266 (Saranya et al., 2018) when cyclones evolved over the BoB passed near their sampling sites.  
267 These results indicate a similar oceanic source of moisture during cyclones. We discuss the  
268 influence of moisture sources in Sect. 4.1.

269 The relation between  $\delta^{18}\text{O}_v$  and  $\delta\text{D}_v$  varies for the periods before, during, and after the cyclones,  
270 showing different slopes and intercepts with the Local Meteoric Vapour Line (LMVL) (Fig. 4).  
271 Before the first event, both the slope (5.85) and intercept (-12.12) are significantly lower  
272 indicating the strong influence of non-equilibrium processes such as evaporation. During both  
273 cyclones the slopes and intercepts resemble those of the global meteoric water line (GMWL:  
274  $\delta\text{D} = 8 \times \delta^{18}\text{O} + 10$ ) (Fig. 4). After the cyclones the slope and intercept decreased to 7.37 and 2.34  
275 respectively, implying a change of moisture sources and evaporation.





276

277 **Figure 4 Relationships between  $\delta^{18}\text{O}_v$  and  $\delta\text{D}_v$  before, during, and after the cyclone events.**

278 **The regression lines for each period are presented along with GMWL for comparison.**

279 **Table 1 Descriptive statistics of  $\delta^{18}\text{O}_v$ ,  $\delta\text{D}_v$ , and d-excess<sub>v</sub> measured before, during, and**

280 **after the cyclone events.**

Period	$\delta^{18}\text{O}_v$ [‰]			$\delta\text{D}_v$ [‰]			d-excess <sub>v</sub> [‰]		
	min	max	avg	min	max	avg	min	max	avg
<b>Before</b>	-12.10	-7.40	-10.04	-84.15	-49.53	-69.51	4.24	15.38	10.84
<b>Cyclone Tauktae</b>	-20.21	-8.20	-14.73	-149.49	-56.06	-106.76	7.97	14.24	11.06
<b>Cyclone Yaas</b>	-24.92	-12.17	-17.87	-183.34	-83.85	-129.18	8.71	18.29	13.77
<b>After</b>	-14.94	-8.29	-11.09	-109.31	-57.40	-79.38	1.80	15.11	9.37

281 To assess the meteorological influence on the isotopic composition at Kathmandu, we examined

282 the linear correlations between the isotopic composition ( $\delta^{18}\text{O}_v$ ,  $\delta\text{D}_v$ , and d-excess<sub>v</sub>), and air

283 temperature (T), relative humidity (RH), precipitation amount (P), wind speed (WS), and dew  
 284 point temperature ( $T_d$ ) before, during, and after the cyclones (Table 2). Before the cyclones, both  
 285  $\delta^{18}O_v$  and  $\delta D_v$  showed a positive correlation with air temperature (i.e., temperature effect) and  
 286 dew point temperature but no correlations with other meteorological variables (Table 2). The  
 287 correlation between  $\delta^{18}O_v/\delta D_v$  and surface air temperature and RH became weaker during the  
 288 cyclone Tauktae while much stronger ( $r=0.60$  for temperature and  $r=-0.68$  for RH) during Yaas.  
 289 During Tauktae, we did not observe any effect of precipitation amount on the isotopic  
 290 composition, while during Yaas there was a negative correlation ( $r=-0.56$ ).  $D\text{-excess}_v$  was  
 291 positively correlated with local air temperature (negatively correlated with local RH) before,  
 292 during, and after Tauktae, whilst no correlations were observed during Yaas (Table 2).

293 **Table 2 Linear correlations between the isotopic composition of atmospheric water vapour**  
 294 **( $\delta^{18}O_v$ ,  $\delta D_v$ , and  $d\text{-excess}_v$ ) and air temperature (T), relative humidity (RH), precipitation**  
 295 **amount (P), wind speed (WS), and dew point temperature ( $T_d$ ) before, during, and after the**  
 296 **cyclone events. \*\*\*, \*\*, and \* indicate correlation significance levels of 0.001, 0.01, and 0.05**  
 297 **respectively.**

	Before				
	T	RH	P	WS	$T_d$
$\delta^{18}O_v$	0.24***	-0.03	-0.41	-0.10	0.51***
$\delta D_v$	0.44***	0.21**	-0.37	0.08	0.63***
$d\text{-excess}_v$	0.66***	-0.64***	0.35	0.68***	0.28***
	Cyclone Tauktae				
$\delta^{18}O_v$	0.15	-0.19	0.11	-0.004	0.07
$\delta D_v$	0.21*	-0.25**	0.10	0.05	0.11
$d\text{-excess}_v$	0.77***	-0.82***	-0.22	0.61***	0.51***
	Cyclone Yaas				
$\delta^{18}O_v$	0.60***	-0.68***	-0.56***	0.02	0.23**
$\delta D_v$	0.63***	-0.70***	-0.56***	0.05	0.26**
$d\text{-excess}_v$	0.10	-0.006	0.19	0.32**	0.26*
	After				

$\delta^{18}\text{O}_v$	0.17*	-0.19*	-	0.19*	0.09
$\delta\text{D}_v$	0.30***	-0.31***	-	0.30***	0.20*
d-excess <sub>v</sub>	0.62***	-0.58***	-	0.52***	0.55***

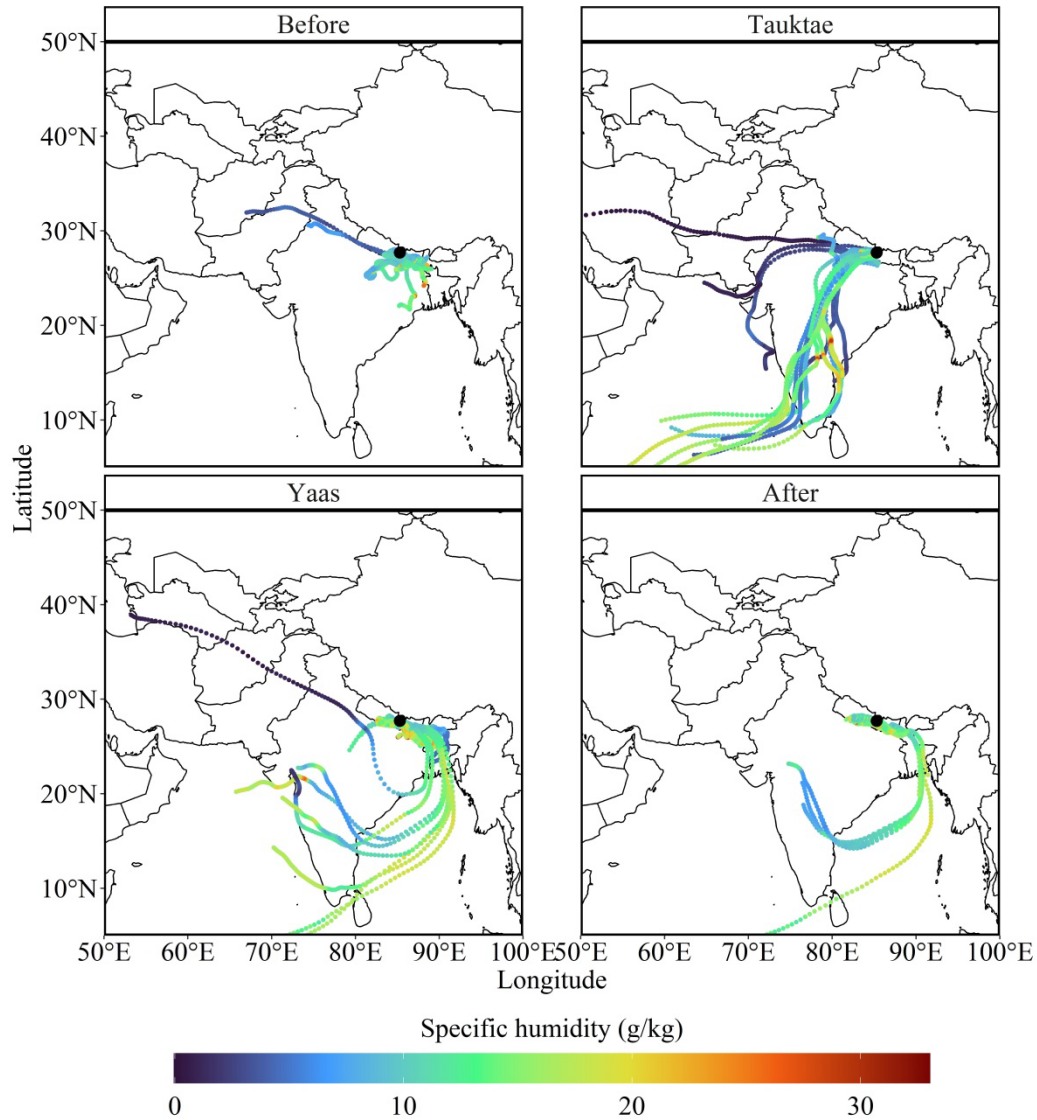
## 298 4 Discussions

299 To investigate the underlying factors behind the isotopic variations, we focused on the impact of  
300 moisture sources, by calculating five-day back trajectories for each day before, during, and after  
301 the cyclone events and changes of corresponding specific humidity. In addition, we explored the  
302 effects of convective activity, moisture convergence, and total rainfall along the back trajectories  
303 on water vapour isotopic depletion.

### 304 4.1 Influence of Moisture source

305 Previous studies suggested that Kathmandu is predominantly impacted by local moisture sources  
306 with short and long-range transport of westerlies before the onset of summer monsoon, which is  
307 generally dry and characterized by sporadic rainfall with enriched  $\delta^{18}\text{O}$  values in precipitation  
308 (Adhikari et al., 2020; Chhetri et al., 2014; Yu et al., 2016). We found significant proportions of  
309 moisture trajectories prior to cyclone Tauktae either originated locally or by westerlies,  
310 characterized by low specific humidity (Fig. 5, upper left panel). These moisture trajectories  
311 were traced back to the Gangetic plain before cyclone Tauktae. The associated  $\delta^{18}\text{O}_v$  and  $\delta\text{D}_v$   
312 values for these moisture sources exhibited enrichment, with average values of -10.04‰ and -  
313 69.51‰ for  $\delta^{18}\text{O}_v$  and  $\delta\text{D}_v$ , respectively. A similar slope (5.85) and intercept (-12.12) of the local  
314 meteoric vapour line before Tauktae to the surface water line calculated in the Gangetic plain  
315 (Hassenruck - Gudipati et al., 2023) which provided corroboration for the impact of local  
316 evaporation on the isotopic composition.

317 As cyclone Tauktae approached the continent, the primary moisture source at Kathmandu  
318 transitioned from local origins to majority AS vapour (Fig. 5, upper right panel). The specific  
319 humidity along these trajectories exhibited higher levels over the oceans, diminishing as they  
320 traversed over land through precipitation (Fig. 5, upper right panel). During this phase,  $\delta^{18}\text{O}_v$  and  
321  $\delta\text{D}_v$  were significantly lower (on average over 4.5‰ and 37‰ for  $\delta^{18}\text{O}_v$  and  $\delta\text{D}_v$  respectively)  
322 than measurements preceding the cyclone. Such depletion can be attributed to the progressive  
323 rainout along the moisture transport path, wherein heavy isotopes are removed during successive  
324 condensation (Xu et al., 2019). Notably, the isotopic composition before the Tauktae-induced  
325 rainfall remained enriched, reflecting inflow from the surface layer (Munksgaard et al., 2015).  
326 Furthermore, the  $d\text{-excess}_v$  variation at Kathmandu during Tauktae may have been influenced by  
327 local moisture recycling processes.



328

329 **Figure 5 Five-day backward moisture trajectories reaching the sampling site before, during,**  
 330 **and after the cyclone events. Colours denote specific humidity ( $q$  in g/kg).**

331 During cyclone Yaas, only the BoB vapour contributed to moisture at Kathmandu and specific  
 332 humidity along the trajectories over the ocean was high (Fig. 5, bottom left panel). The high  
 333 specific humidity over India and surrounding regions during cyclone formation suggest that Yaas  
 334 lifted a substantial amount of water vapour from the BoB yielding intense rainfall along its path.  
 335 The isotopic composition during Yaas was more depleted than that of Tuaktae with averages of -

336 17.87‰ and -129.18‰ for  $\delta^{18}\text{O}_v$  and  $\delta\text{D}_v$  respectively. The difference could stem from varied  
337 moisture sources, rainout histories, and the respective strengths of each cyclone. Moreover, the  
338 high isotopic depletion during cyclone Yaas might be attributed to the disparity of sea surface  
339 water  $\delta^{18}\text{O}$  between the AS and BoB. The surface water  $\delta^{18}\text{O}$  in the BoB is relatively depleted  
340 compared to the AS (Lekshmy et al., 2014), which results from a substantial influx of freshwater  
341 from rain and runoff originating from the Ganga Brahmaputra river basin (Breitenbach et al.,  
342 2010; Singh et al., 2010).

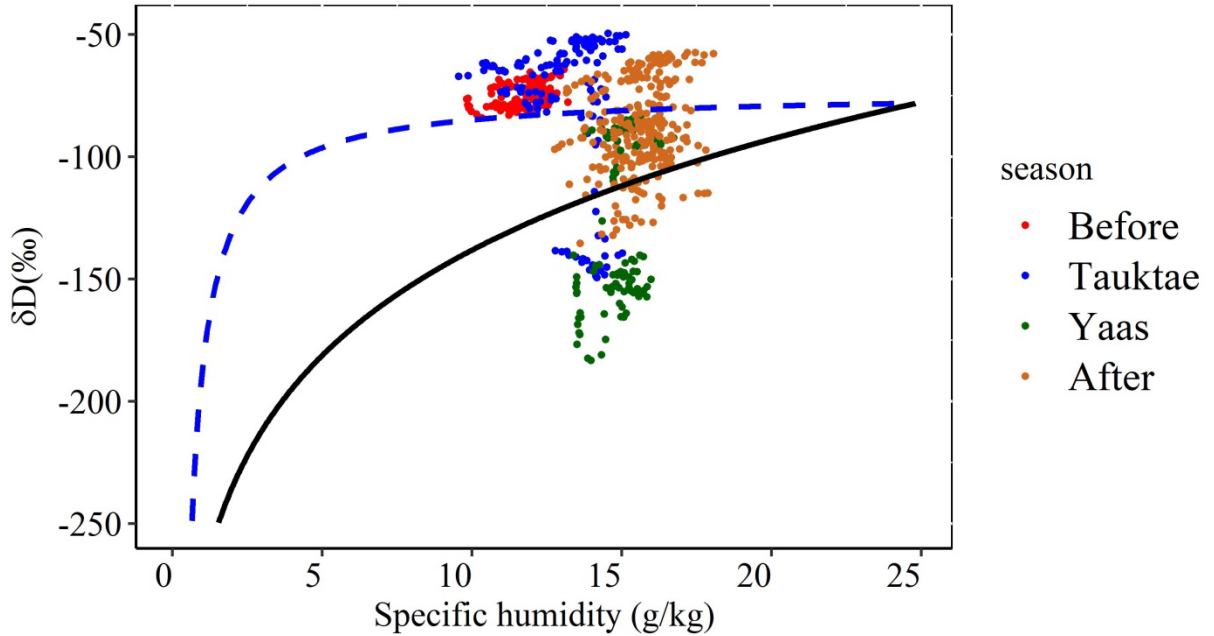
343 Although, the progressive increment was seen in the time series of  $\delta^{18}\text{O}_v$  and  $\delta\text{D}_v$  after the  
344 dissipation of Tauktae (Fig. 3),  $\delta^{18}\text{O}_v$  and  $\delta\text{D}_v$  in the earlier stage of Yaas were significantly  
345 lower compared to Tauktae because there was not enough time for recovery. There was a strong  
346 association between  $\delta^{18}\text{O}_v$ /or  $\delta\text{D}_v$  and local meteorological conditions during cyclone Yaas  
347 associated with high relative humidity from the remote ocean (Chen et al., 2021; Xu et al., 2019).  
348 Furthermore, the negative correlation of  $\delta^{18}\text{O}_v/\delta\text{D}_v$  vs. RH and the fact that  $\delta^{18}\text{O}_v/\delta\text{D}_v$  was  
349 depleted highlight the influence of humid moisture sources (Yu et al., 2008), which was also  
350 confirmed by our moisture back trajectory analysis (Fig. 5, bottom left panel). A similar  
351 correlation was also observed in mid-tropospheric water vapour over the western Pacific  
352 associated with intense convective activity (Noone, 2012).

353 In contrast to cyclone Tauktae, the lack of correlation of  $d\text{-excess}_v$  with RH and local air  
354 temperature during cyclone Yaas implies that local moisture recycling processes are not  
355 significant in determining  $d\text{-excess}_v$  variation and RH might not be a reliable predictor of kinetic  
356 fractionation during evaporation. Previous research conducted in the Indian Ocean (e.g., Midhun  
357 et al., 2013; Uemura et al., 2008) suggested that the high relative humidity (i.e. >80%) at the  
358 sampling sites weakens the correlation between  $d\text{-excess}_v$  and RH. Our observed data also

359 satisfied that condition during Yaas because the majority of isotopic measurements (about 75%)  
360 were associated with high relative humidity (>80%), while this fraction was only 25% during  
361 Tauktae.

362 Following the dissipation of the cyclones, some moisture at Kathmandu was provided by BoB  
363 vapour together with local evaporation (Fig. 5, bottom right panel). However, the isotopic  
364 composition reverted to the original (enriched) levels ( $\delta^{18}\text{O}_v = -11.09 \text{ ‰}$ ,  $\delta\text{D}_v = -79.38 \text{ ‰}$ , and  $d\text{-}$   
365  $\text{excess}_v = 9.37 \text{ ‰}$ ). The diminished correlation between  $\delta^{18}\text{O}_v/\delta\text{D}_v$  and temperature following the  
366 cyclones is attributed to the admixture of vapour originating from plant transpiration during that  
367 period (Delattre et al., 2015).

368 We used the vapour  $\delta\text{D}_v$ - $q$  plot combined with the Rayleigh distillation and mixing curve to  
369 assess the moisture mixing (Fig. 6). Before the development of cyclone Tauktae and during its  
370 early stages, the data points lie well above the mixing curve, indicating that the isotopic  
371 variability was mainly dominated by vapour from local evapotranspiration. In contrast, during  
372 the latter stage of cyclone Tauktae,  $\delta\text{D}_v$  was significantly depleted to levels well below the  
373 Rayleigh curve. During the early stage of cyclone Yaas, there are only a few data points between  
374 the mixing and Rayleigh curves with the majority well below the Rayleigh curve, particularly  
375 during the later stage. During both events, Kathmandu was dominated by deep convection  
376 leading to a strong convergence of moisture from both the AS (Tauktae) and the BoB (Yaas).  
377 This points towards the influence of convective processes (see Section 4.2) (Galewsky and  
378 Samuels-Crow, 2015). After Yaas had dissipated,  $\delta\text{D}_v$  gradually increased again with half of the  
379 data points clustered between the mixing and Rayleigh curves. The remaining data points were  
380 well above the mixing curve, indicating the influence of locally evaporated vapour also  
381 evidenced by the moisture back trajectories (Fig. 5 bottom right panel).



382

383 **Figure 6 Scatter plot of hourly averaged  $\delta D_v$  vs. specific humidity (q). The solid black curve**  
 384 **represents the Rayleigh distillation curve calculated for the initial condition of  $\delta D_v =$**   
 385  **$-78.20$  ‰, BoB-averaged  $\delta D_v$  (Lekshmy et al., 2022), SST of  $30^\circ$  C, and RH of 90 %. The**  
 386 **dashed blue curve represents the mixing line, calculated based on dry continental air (q=**  
 387  **$0.5$  g/kg and  $\delta D_v = -300$  ‰ (Wang et al., 2021)) and the wet source, which corresponds to the**  
 388 **initial conditions used to calculate the theoretical Rayleigh curve.**

#### 389 **4.2 Influence of deep convection associated with cyclones**

390 One of the likely causes for large isotopic depletion during cyclones might be the associated  
 391 convective processes. Studies have demonstrated that convective processes within tropical  
 392 cyclones can cause the depleted isotopic composition of precipitation and atmospheric water  
 393 vapour (Fudeyasu et al., 2008; Jackisch et al., 2022; Munksgaard et al., 2015) due to a  
 394 combination of strong cyclonic circulation, intense large-scale convection, heavy precipitation,  
 395 and high wind speeds (Chen et al., 2021; Xu et al., 2019). We analysed the relationship between



396 the isotopic composition and convective processes, using OLR and vertical velocity as a proxy  
397 for convection. Due to the frequent co-occurrence of intense convection and significant mid-  
398 tropospheric convergence of moist air, the vertical velocities can also serve as a proxy for  
399 convective activity (Lekshmy et al., 2014).

400 Fig. S3 and Fig. S4 depict the prevalence of strong convective processes associated with both  
401 cyclones throughout their lifespan. During the initial days of cyclone formation, OLR exceeded  
402  $260 \text{ Wm}^{-2}$  in the area of the sampling site and decreased rapidly to below  $200 \text{ Wm}^{-2}$  in the final  
403 stages of both cyclones when approaching the site. Although the amount of precipitation  
404 associated with Tauktae (9.2 mm) was much lower than Yaas (59.6 mm),  $\delta^{18}\text{O}_v$  depleted by up to  
405 12 ‰ during both cyclones. The progressive rainout was evident along the entire cyclone track,  
406 and the spatial distribution of precipitation was highly correlated with the convective process, as  
407 indicated by low OLR (Figs. S5 and S6), suggesting rainfall occurred from the deep convective  
408 cloud rather than local evaporation. This was confirmed by precipitation variations. The site  
409 received its first rainfall on 19 May during cyclone Tauktae and on 25 May during cyclone Yaas,  
410 as shown in Figure S5 and Figure S6. *In situ* observations confirm that during the days leading  
411 up to cyclone Tauktae, the sampling site received a total of 12.2 mm of precipitation with  
412 maximum rainfall of 9.2 mm/h recorded on 11 May at 13:00 h LT, equal to the total accumulated  
413 rainfall during the entire cyclone. Although the pre and during-Tauktae rainfall amounts are  
414 similar, pre-cyclone  $\delta^{18}\text{O}_v$  and  $\delta\text{D}_v$  were significantly more enriched (averages:  $\delta^{18}\text{O}_v = -10.04 \text{ ‰}$   
415 and  $\delta\text{D}_v = -69.51 \text{ ‰}$ ) than during Tauktae (averages:  $\delta^{18}\text{O}_v = -14.73 \text{ ‰}$  and  $\delta\text{D}_v = -106.76 \text{ ‰}$ ).  
416 We compared the values of  $\delta^{18}\text{O}_v$ ,  $\delta\text{D}_v$ , and  $d\text{-excess}_v$  during both events and also examined  
417 them in comparison with the isotopic composition at the beginning of the summer monsoon  
418 (June 2021). This initial period of intense and continuous rainfall at our sampling site (Fig. S7) is

419 regulated by the monsoon system originating in the BoB. Consequently, our focus centered on  
420 the isotopic distinctions between water vapour on typical rainy days and that associated with  
421 cyclone Yaas.

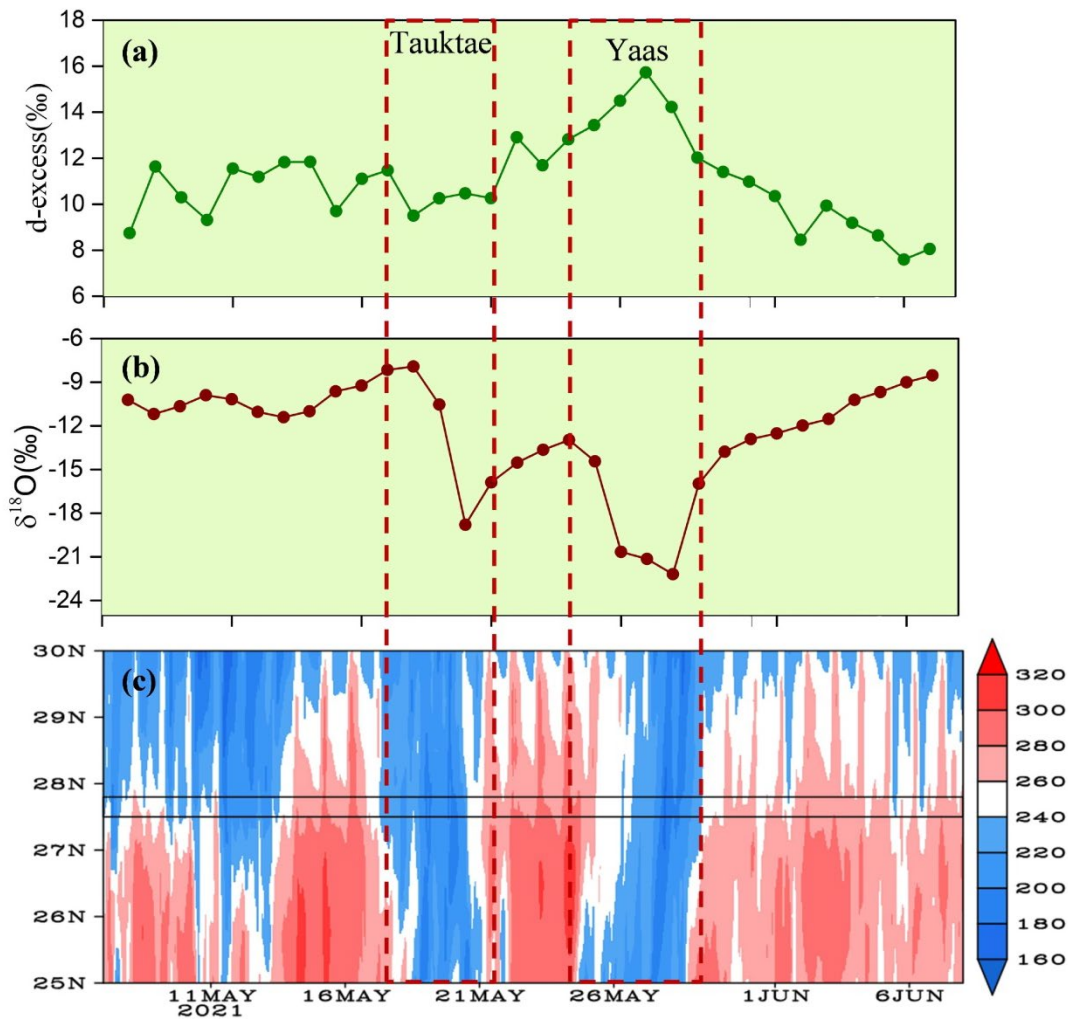
422 Following the initiation of the summer monsoon, both  $\delta^{18}\text{O}_v$  and  $\delta\text{D}_v$  exhibited a progressive  
423 depletion, coinciding with a decline in air temperature, an increase in relative humidity (RH),  
424 and amplified rainfall amounts (Fig. S7). Despite the daily accumulated rainfall and RH being  
425 significantly higher during the normal monsoon period, both  $\delta^{18}\text{O}_v$  and  $\delta\text{D}_v$  were markedly lower  
426 during cyclone Yaas (on average by over 2.5‰ and 26‰ for  $\delta^{18}\text{O}_v$  and  $\delta\text{D}_v$  respectively)  
427 compared to typical rainy days. A progressive reduction in  $d\text{-excess}_v$  was also evident as the  
428 summer monsoon unfolded; a trend typically observed in precipitation  $d\text{-excess}$  (e.g., Hussain et  
429 al., 2015; Acharya et al., 2020; Adhikari et al., 2020) and water vapour  $d\text{-excess}$  (Tian et al.,  
430 2020; Yao et al., 2018; He and Richards, 2016; Wei et al., 2016) in Asian monsoon regions, in  
431 contrast to our observations during cyclone Yaas.

432 Given that  $d\text{-excess}$  has long served as a diagnostic tool for understanding moisture source  
433 conditions (Tian et al., 2001; Liu et al., 2008), the distinct behaviour of  $d\text{-excess}_v$  between  
434 cyclone Yaas and the normal monsoon phase suggests that cyclone-related information may be  
435 discerned through the isotopic composition recorded at our site. This confirms our previously  
436 stated hypothesis that rainfall associated with cyclones causes significantly lower isotope values  
437 in vapour due to intense convective systems (Gedzelman et al., 2003; Kurita, 2013), absent in  
438 local rain events and days without precipitation (Lekshmy et al., 2022).

439 The influence of convective processes on water vapor isotopic variations at Kathmandu is further  
440 supported by the Hovmöller diagram of OLR averaged over 80-90° E, which clearly shows that

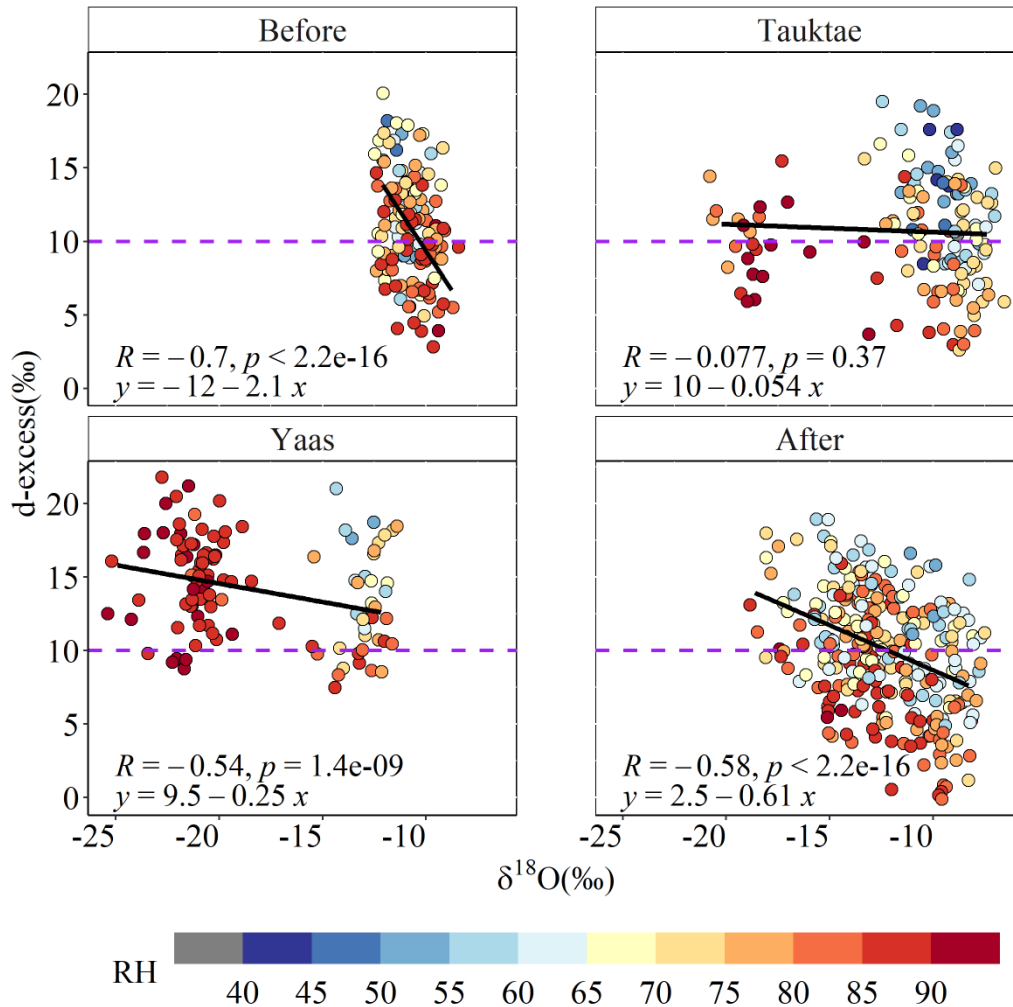
441  $\delta^{18}\text{O}_v$  depletion coincides with the presence of clouds (Fig. 7a and c). In contrast,  $d\text{-excess}_v$   
442 showed dissimilar variations between both cyclones. Before cyclone Tauktae, the daily averaged  
443  $d\text{-excess}_v$  was above the global average of 10 ‰ (Fig. 7a). Once Tauktae approached our  
444 sampling site,  $d\text{-excess}_v$  decreased from around 12 ‰ to 10 ‰ and continued to oscillate about  
445 10 ‰ until Tauktae had dissipated. As cyclone Yaas approached the measurement site with  
446 intense rainfall (Fig. 3),  $d\text{-excess}_v$  gradually increased while RH increased, and air temperature  
447 decreased (Fig. 3). Specifically,  $d\text{-excess}_v$  on 24 May was recorded as 12.82 ‰ when surface air  
448 temperature and surface RH was about 24 °C and 70 % respectively. On 27 May, we noted a 3 ‰  
449 rise in  $d\text{-excess}_v$  when the surface temperature was reduced by 4 °C and the surface RH was  
450 increased by 19 %. The combination of increasing  $d\text{-excess}$  and decreasing  $\delta^{18}\text{O}_v$  highlights the  
451 role of vapour recycling due to the subsidence of air masses from stratiform clouds (Kurita et al.,  
452 2011). In addition, a large increase in  $d\text{-excess}_v$  was also recorded in atmospheric vapour during  
453 cyclone Ita in 2014 and was attributed to downward moisture transport above the boundary layer  
454 (Munksgaard et al., 2015). We did not find any statistically significant correlation during cyclone  
455 Yaas between  $d\text{-excess}_v$  and RH/Temperature, although RH is considered an important  
456 parameter for interpreting  $d\text{-excess}$  in atmospheric vapour and precipitation (Pfahl and  
457 Sodemann, 2014; Steen-Larsen et al., 2014). The observed co-occurrence of higher  $d\text{-excess}_v$ ,  
458 lower temperatures, and high relative humidity (Fig. 3) points to kinetic fractionation processes  
459 either at a larger scale or in association with downdrafts (Conroy et al., 2016). Rain re-  
460 evaporation under the condition of high saturation deficit is one of the causes of low  $\delta^{18}\text{O}_v$  and  
461 high  $d\text{-excess}_v$ . This is due to the addition of re-evaporated vapour during precipitation events,  
462 which results in depleted cloud vapour and high  $d\text{-excess}_v$  (Conroy et al., 2016; Lekshmy et al.,  
463 2014). On normal days high  $d\text{-excess}_v$  values were generally accompanied by low RH (Fig. 8)

464 and vice versa. However, the high relative humidity of the surface air together with near  
 465 saturation conditions vertically (Fig. 9b) during cyclone Yaas, rule out any effect of re-  
 466 evaporation on increased  $d\text{-excess}_v$  values. Such high  $d\text{-excess}_v$  values may be associated with  
 467 downdrafts during convective rain events, transporting isotopically depleted vapour with higher  
 468  $d\text{-excess}_v$  values from the boundary layer to the surface (Kurita, 2013; Midhun et al., 2013).



469

470 **Figure 7** Time series of daily averaged  $d\text{-excess}_v$  (a),  $\delta^{18}\text{O}_v$  (b), and Hovmöller diagram of  
 471 **OLR ( $\text{W}/\text{m}^2$ ) averaged over  $80^\circ \text{E}-90^\circ \text{E}$  (c)** The solid parallel lines in (c) depict the latitude  
 472 **range of sampling site.**



473

474 **Figure 8 Scatter plots of  $d\text{-excess}_v$  vs.  $\delta^{18}\text{O}_v$  before, during, and after the cyclone events.**

475 **The colour represents RH (in %) and the horizontal dashed purple lines represent the**

476 **global average d-excess value (10 ‰).**

477 To clarify the impact of convection on the isotopic composition, we analysed the distribution of

478 vertical velocity, relative humidity, and air temperature averaged over a box between  $25^\circ\text{N}$ - $28^\circ\text{N}$

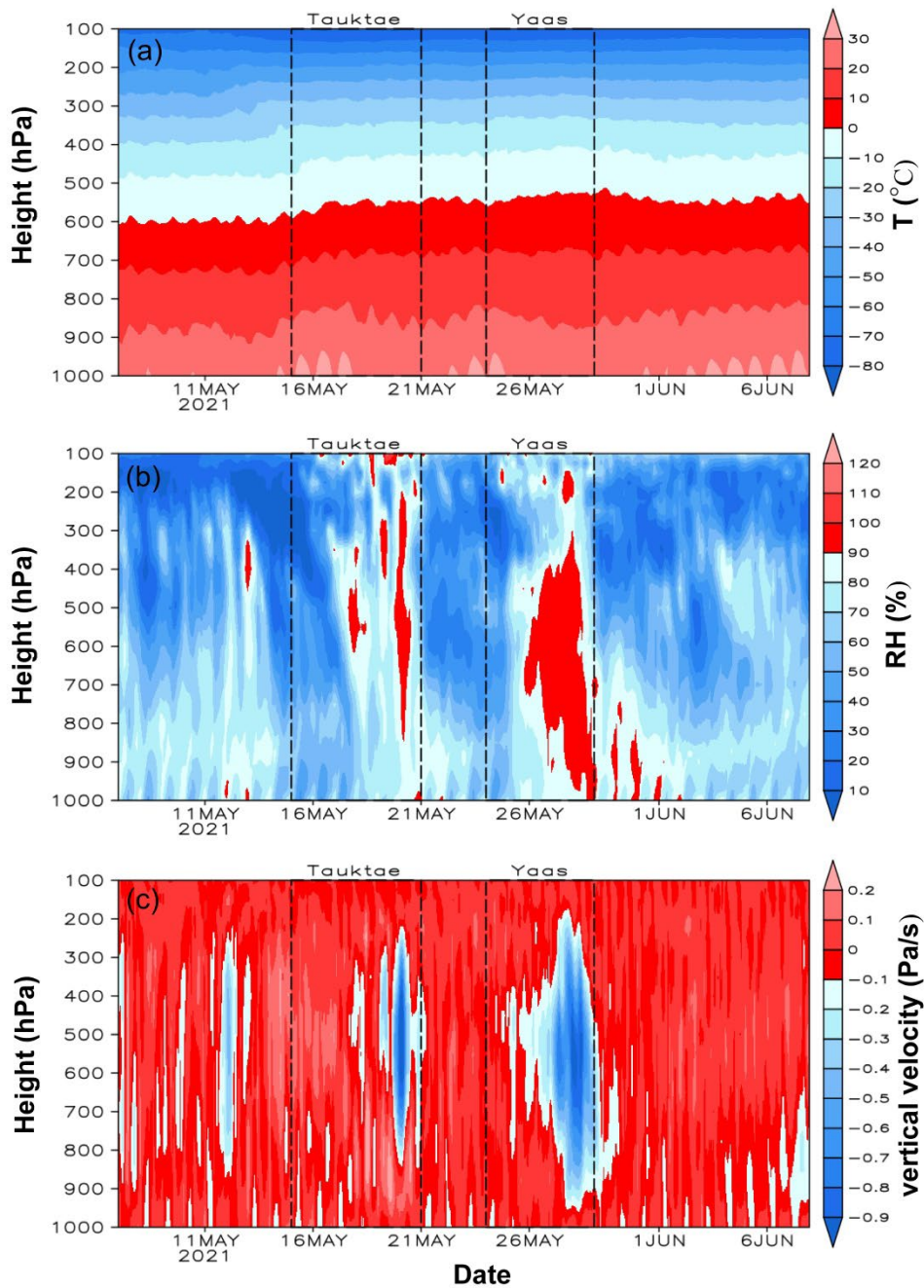
479 and  $83^\circ\text{E}$ - $87^\circ\text{E}$  with our measurement site near its center (Fig. 9). Our results show that strong

480 shifts in  $\delta^{18}\text{O}_v$ ,  $\delta D_v$ , and  $d\text{-excess}_v$  during the cyclones were strongly associated with vertical air

481 motions (Fig. 9c). We observed a general downward movement of air before the rain started with

482 Tauktae. The high depletion of  $\delta^{18}\text{O}_v$  and  $\delta\text{D}_v$  during the final stages of Tauktae (Fig. 3) was  
483 accompanied by strong upward air movement extending from 800 hPa to about 200 hPa (Fig. 9c).  
484 This upward motion was even stronger during cyclone Yaas and became evident near the  
485 measurement site once Yaas made landfall on 26 May. Interestingly, variations in RH at different  
486 pressure levels strongly coincided with changes in vertical velocity while the lower troposphere  
487 remained near saturation (RH= ~100 %) during the final stages of both cyclones (Fig. 9b). While  
488 the air temperature showed the expected decline with altitude (Fig. 9a), there were no significant  
489 temporal variations during the entire period, despite the high variation in RH. The strong  
490 convective updraft added additional moisture from the warm ocean below, before passing over  
491 our measurement site (Lekshmy et al., 2014). Convective updrafts cause moisture to condense  
492 quickly and this high-efficiency condensation of heavy rain can result in more depleted  $\delta^{18}\text{O}_v$   
493 and  $\delta\text{D}_v$  (Lawrence and Gedzelman, 1996). In addition, we found a strong positive correlation  
494 between  $\delta^{18}\text{O}_v$  and average vertical velocity ( $r=0.57$ ) during Yaas at pressure levels between 300  
495 hPa and 600 hPa (Fig. S8a) in the area surrounding our site. This correlation was weaker ( $r=0.30$ )  
496 during Tauktae. The distinctive relationship between  $\delta^{18}\text{O}_v$  and vertical velocity implies that  
497 convective processes play a more significant role during Yaas than Tauktae. This result was  
498 further supported by the spatial distribution of correlation coefficient between  $\delta^{18}\text{O}_v$  and vertical  
499 velocity (Fig. S8b, c). During cyclone Tauktae, a significant negative correlation was observed  
500 between  $\delta^{18}\text{O}_v$  and vertical velocity around the sampling site, while positive correlation areas  
501 were identified in western Nepal, certain parts of central India, and the coastal region of the Bay  
502 of Bengal (BoB) (Fig. S8b). A comparison with back trajectories unveiled positive correlation  
503 only in specific sections along the moisture transport path, suggesting that convective processes  
504 may not be the primary driver of isotopic depletion during cyclone Tauktae. Conversely, a

505 positive correlation was evident in the coastal BoB, extending north toward the sampling site  
506 during cyclone Yaas (Fig. S8c). The positive correlation areas were considerably larger  
507 compared to Tauktae, and these areas closely aligned with the moisture transport path. Hence,  
508 higher depletion in  $\delta^{18}\text{O}_v$  and  $\delta\text{D}_v$  during Yaas, relative to Tauktae, may be attributed to the  
509 stronger convection associated with BoB vapour compared to the AS vapour. The BoB is a  
510 convectively active region, and previous studies reported greater depletions in  $\delta^{18}\text{O}$  and  $\delta\text{D}$  in  
511 precipitation, irrespective of the season (Breitenbach et al., 2010; Lekshmy et al., 2015; Midhun  
512 et al., 2018). Another reason we observed different levels of isotope depletion between both  
513 cyclones may be related to differences in their proximity to the sampling site. While Yaas came  
514 as close as 400 km to our site, Tauktae was 1100 km away when it dissipated (Fig. S9). The  
515 proximity of Yaas may explain the stronger rainfall during that event which enhanced the  
516 isotopic fractionation in turn leading to stronger isotopic depletion (Jackisch et al., 2022). Similar  
517 results have been documented for precipitation stable isotopes (e.g., Fudeyasu et al., 2008;  
518 Jackisch et al., 2022; Munksgaard et al., 2015; Xu et al., 2019) and water vapour stable isotopes  
519 (e.g., Munksgaard et al., 2015; Rahul et al., 2016; Saranya et al., 2018). Even after both cyclones  
520 had dissipated, progressive rainfall continued at our sampling site due to the presence of residual  
521 moisture from the cyclones. Once these residual effects had diminished and rainfall intensity  
522 weakened,  $\delta^{18}\text{O}_v$  and  $\delta\text{D}_v$  started to increase again (Fig. 3), likely due to evaporative effects  
523 (Munksgaard et al., 2015; Xu et al., 2019; Jackisch et al., 2022).



524

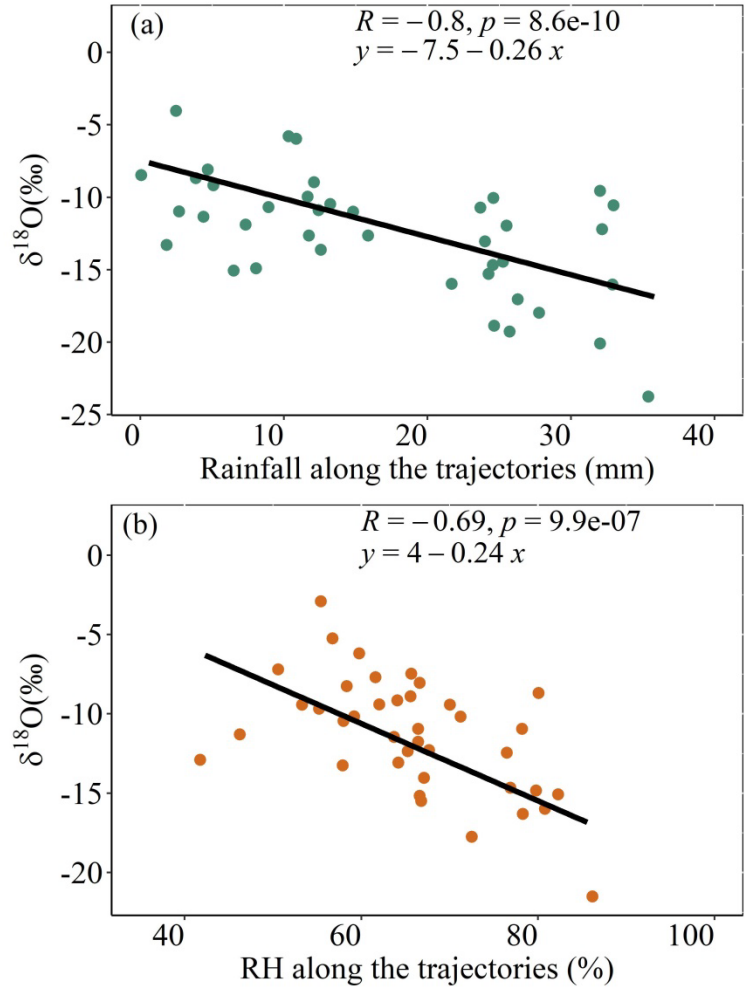
525 **Figure 9 Time series of the vertical distribution of air temperature (a), RH (b), and vertical**  
 526 **velocity (c) averaged over 25° N-28° N and 83° E-87° E with Kathmandu approximately at**  
 527 **the centre. Negative (positive) vertical velocities indicate ascending (descending) winds.**



### 528 **4.3 Influence of rainfall**

529 The back trajectories reveal the impact of separate air masses during cyclones Tauktae and Yaas,  
530 specifically between the AS and BoB. We studied the meteorological conditions along the 5-day  
531 moisture back trajectories, focusing on the upstream rainout on observed isotopic depletion.  
532 During cyclone Tauktae, both  $\delta^{18}\text{O}_v$  and  $\delta\text{D}_v$  display a strong negative correlation ( $r = -0.80$  and  
533  $r = -0.79$  for  $\delta^{18}\text{O}_v$  and  $\delta\text{D}_v$ , respectively, Fig. 10) with total precipitation along the moisture  
534 trajectories (i.e., upstream rainout). Moreover, a negative correlation emerges between  $\delta^{18}\text{O}_v/\delta\text{D}_v$   
535 and average relative humidity (RH) along the trajectories ( $r = -0.69$  for  $\delta^{18}\text{O}_v$  and  $-0.68$  for  $\delta\text{D}_v$ ),  
536 suggesting increased upstream rainout corresponds to lower isotope ratios during cyclone  
537 Tauktae.

538 In addition, modelled back trajectories indicate that air masses during cyclone Tauktae had a  
539 longer transport time when continuous rainout could have enhanced the isotopic depletion of the  
540 residual vapour (Fig. 5b). The upstream rainfall control could also account for the delayed return  
541 of  $\delta^{18}\text{O}_v$  and  $\delta\text{D}_v$  to more positive values following dissipation.



542

543 **Figure 10 (a) Scatter plots of  $\delta^{18}\text{O}_v$  vs upstream rainout and (b) average relative humidity**

544 **(RH) along the moisture trajectories during the cyclone Tauktae.**

545 Similar observations have been documented in other regions; for example, the Chinese Typhoons

546 Haitang, Megi, and Soudelor (Xu et al., 2019), the Central American Hurricanes Irma and Otto

547 (Sánchez-Murillo et al., 2019), and Central Texas Hurricane Harvey (Sun et al., 2022) all

548 demonstrate significant negative correlations between upstream rainout and precipitation  $\delta^{18}\text{O}$ .

549 This suggests that upstream rainout could serve as a widely applicable control on the

550 spatiotemporal variability in tropical cyclones (Sun et al., 2022).

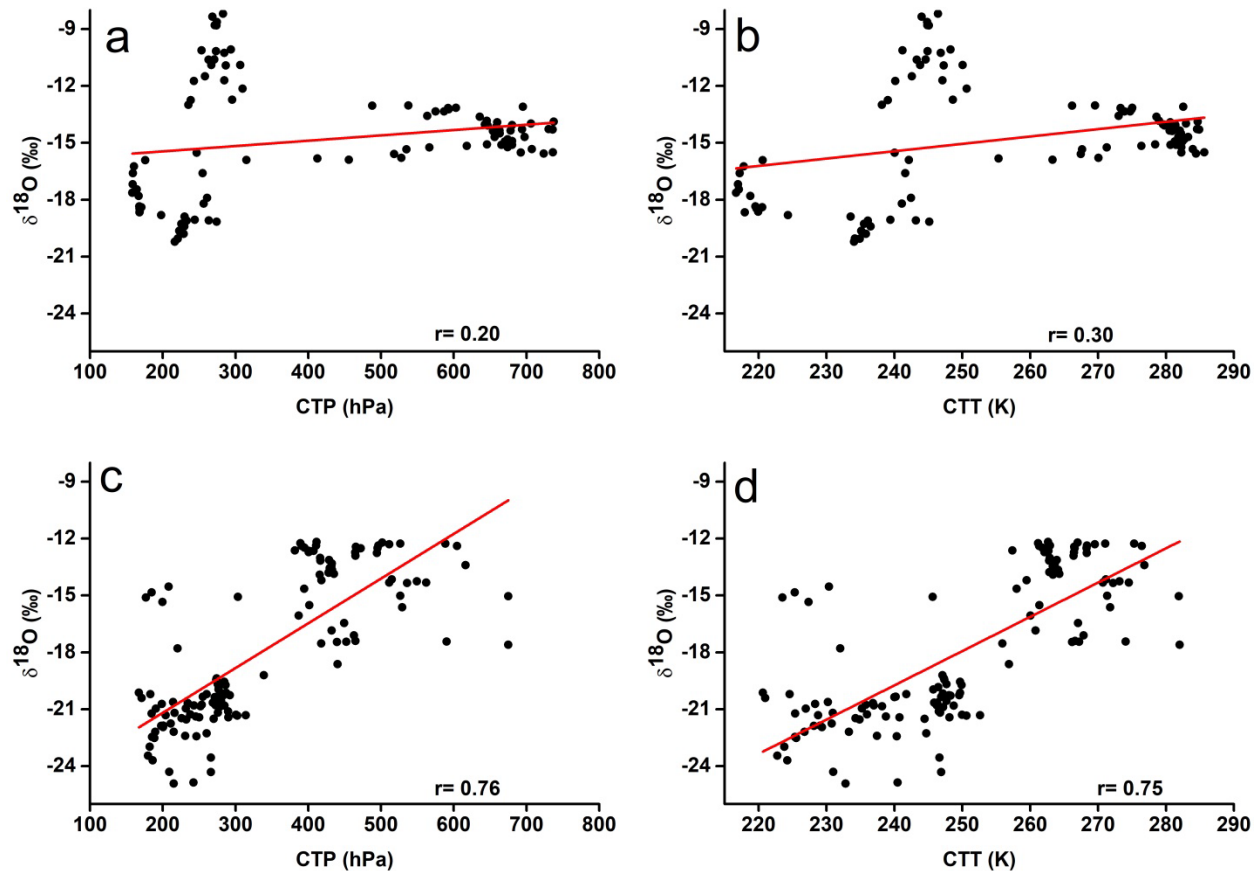
551 In contrast to cyclone Tauktae, neither the total rainfall nor the relative humidity (RH) along the  
552 trajectories appears to exert influence on isotopic variation during cyclone Yaas. Instead, a  
553 negative correlation was observed between  $\delta^{18}\text{O}_v/\delta\text{D}_v$  and local rainfall amount, air temperature,  
554 and RH (Table 2). This suggests that the observed isotopic depletion during cyclone Yaas cannot  
555 be adequately explained by upstream rainout processes. We assume that sudden changes in local  
556 meteorological conditions are a consequence of synoptic processes during the cyclones. The  
557 progressive rainout during the cyclone events followed a temperature decrease (Figure 2) which  
558 would result in the  $\delta^{18}\text{O}_v/\delta\text{D}_v$  correlation with temperature (Delattre et al., 2015). The cooling of  
559 surface air during rainfall, coupled with the isotopic equilibrium of vapour with raindrops,  
560 establishes a positive correlation between  $\delta^{18}\text{O}_v/\delta\text{D}_v$  and temperature (Midhun et al., 2013).  
561 These conditions were favourable during cyclone Yaas because the sampling site experienced  
562 consistent rainfall, along with a noticeable increase in relative humidity and a decrease in  
563 temperature. This might be one of the reasons for the weaker correlation of  $\delta^{18}\text{O}_v/\delta\text{D}_v$  with local  
564 meteorological variables during Tauktae.

565 Studies have speculated that the impact of precipitation amount is not confined to a strictly local  
566 context (Galewsky et al., 2016), but is subject to modulation by convective and large-scale  
567 atmospheric properties including downdraft moisture recycling (Risi et al., 2008), large-scale  
568 organized convection and associated stratiform rain (Kurita, 2013), as well as regional  
569 circulation and shifting moisture sources (Lawrence et al., 2004). Our measurements during  
570 cyclone Yaas revealed the presence of an intense convective system over our study site,  
571 indicating that the observed effect of rainfall amount may have been governed by moisture  
572 convergence (Chakraborty et al., 2016). The subsequent rainfall originating from the convective  
573 system, occurring over a region characterized by depleted isotope values, resulted in a negative

574 association between precipitation amount and  $\delta^{18}\text{O}_v/\delta\text{D}_v$  (Kurita, 2013). The  $^{18}\text{O}$ -depleted water  
575 vapour reaching the sub-cloud layer, accompanied by the intense convective downdrafts,  
576 subsequently ascended back to the cloud level with the updrafts, in a feedback mechanism  
577 proposed by Lekshmy et al., (2014).

578 Given that CTT and CTP are reliable indicators of both moisture convergence and convective  
579 strength in prior studies (Cai et al., 2018; Cai and Tian, 2016), we investigate the linear  
580 correlation between CTT/CTP (averaged over the  $27^\circ\text{N}$ - $28^\circ\text{N}$  latitude and  $85^\circ\text{E}$ - $86^\circ\text{E}$  longitude  
581 range, with our site located at the center) and  $\delta^{18}\text{O}_v$  (Fig. 11). The results demonstrate a weak  
582 positive correlation between CTT/CTP and  $\delta^{18}\text{O}_v$  during cyclone Tauktae, and a robust positive  
583 correlation during cyclone Yaas. These correlations exhibit greater strength compared to the  
584 correlation observed with local rainfall. Previous research has highlighted positive correlations  
585 between  $\delta^{18}\text{O}$  and CTT/CTP in the East Asian Monsoon suggesting that intense convection and  
586 moisture convergence lead to an increase in cloud-top height and a decrease in CTT, causing a  
587 reduction in  $\delta^{18}\text{O}$  (Cai and Tian, 2016). The decrease in  $\delta^{18}\text{O}_v$  during cyclone Yaas coupled with  
588 a decrease in CTT and CTP (i.e. increase in cloud-top height), shows the influence of intensified  
589 convective activities and moisture convergence, while the isotopic depletion during cyclone  
590 Tauktae is attributed to upstream rainout processes. Furthermore, a negative correlation is  
591 evident between  $d\text{-excess}_v$  and CTT/CTP, with  $r = -0.52$  and  $r = -0.60$  during cyclone Yaas.  
592 Conversely, a weak positive correlation is observed during cyclone Tauktae, with  $r = 0.32$  for  
593 both CTT and CTP. This relationship implies that lower CTT and CTP during intense convection  
594 relate to increased  $d\text{-excess}_v$  values during the final stage of cyclone Yaas.

595



596

597 **Figure 11 Relationship between hourly  $\delta^{18}\text{O}_v$  and (a) CTT during Tauktae, (b) CTP during**  
 598 **Tauktae, (c) CTT during Yaas, and (d) CTP during Yaas.**

## 599 **5 Conclusion**

600 This study presented the results of continuous measurements of the isotopic composition of  
 601 atmospheric water vapour over Kathmandu between 7 May and 7 June 2021 covering two  
 602 cyclone events; cyclone Tauktae formed over the Arabian Sea, and cyclone Yaas formed over  
 603 the Bay of Bengal.  $\delta^{18}\text{O}_v$  ( $\delta\text{D}_v$ ) during Tauktae varied from  $-8.20\text{‰}$  ( $-56.06\text{‰}$ ) to  $-20.21\text{‰}$  ( $-$   
 604  $149.49\text{‰}$ ) with an average of  $-14.73\text{‰}$  ( $-106.76\text{‰}$ ) and during Yaas  $\delta^{18}\text{O}_v$  ( $\delta\text{D}_v$ ) ranges from  $-$   
 605  $12.17\text{‰}$  ( $-83.85\text{‰}$ ) to  $-24.92\text{‰}$  ( $-183.34\text{‰}$ ) with an average of  $-17.87\text{‰}$  ( $-129.18\text{‰}$ ). Similarly,  
 606  $d\text{-excess}_v$  during Tauktae varied from  $7.97\text{‰}$  to  $14.24\text{‰}$  with an average of  $11.06\text{‰}$  while

607 during Yaas it varied from 8.71 ‰ to 18.29 ‰ with an average of 13.77 ‰. Both cyclones led to  
608 significant depletion of  $\delta^{18}\text{O}_v$  and  $\delta\text{D}_v$ , with  $\delta^{18}\text{O}_v$  decreasing by over 12 ‰. We attribute these  
609 rapid depletions to changes in moisture sources (local vs. marine) inferred from backward  
610 moisture trajectories. The lower intercepts of the local meteoric vapour line before and after the  
611 events highlight the influence of non-equilibrium processes such as evaporation on the isotopic  
612 composition. The spatial distribution of OLR, vertical velocity, and regional precipitation during  
613 both cyclonic events indicated significant moisture convergence and intense convection at and  
614 around the measurement site. This resulted in depleted  $\delta^{18}\text{O}_v$  and  $\delta\text{D}_v$ , with cyclone Yaas  
615 exhibiting stronger moisture convergence and convection, leading to lower  $\delta^{18}\text{O}_v$  values  
616 compared to cyclone Tauktae. This difference may be attributed to robust downdrafts during  
617 Yaas-related convective rain events, potentially transporting vapour with higher d-excess<sub>v</sub> and  
618 lower  $\delta^{18}\text{O}_v$  values to the surface. The observed isotopic depletion during cyclone Tauktae can be  
619 explained by upstream rainout processes, unlike during Yaas.

620 Overall, our results show that tropical cyclones originating in the BoB and the AS during the pre-  
621 monsoon season transport large amounts of isotopically depleted vapour and produce moderate  
622 to heavy rainfall over a sizeable region in Nepal. The isotopic composition of atmospheric water  
623 vapour and precipitation during the dry season should therefore be interpreted with caution, and  
624 the effects of cyclones should not be underestimated. In addition, our results underline the need  
625 for simultaneous measurements of the isotopic composition of both atmospheric water vapour  
626 and precipitation to better understand post-condensation exchanges between falling raindrops  
627 and boundary layer vapour over Kathmandu.

628

629 **Data Availability**

630 The data used in this study will be available in the Zenodo repository.

631 **Competing interests**

632 The contact author has declared that none of the authors has any competing interests.

633 **Acknowledgements**

634 This work was funded by ‘The Second Tibetan Plateau Scientific Expedition and Research  
635 (STEP) project’ (Grant No. 2019QZKK0208) and the National Natural Science Foundation of  
636 China (Grants 41922002 and 41988101-03). We thank Yulong Yang for his assistance with  
637 instrument set-up and initial running.

638 **Author contributions**

639 **Niranjan Adhikari**: Data curation, Formal analysis, Writing - Original draft preparation. **Jing**  
640 **Gao**: Data curation, Conceptualization, Methodology, Supervision, Writing - Review and  
641 Editing, Funding acquisition. **Aibin Zhao**: measuring assistance, Writing – Editing. **Tianli Xu**,  
642 **Manli Chen**, and **Xiaowei Niu**: measuring assistance. **Tandong Yao**: Supervision, Funding  
643 acquisition.

644 **6 References**

- 645 Acharya, S., Yang, X., Yao, T., Shrestha, D.: Stable isotopes of precipitation in Nepal Himalaya  
646 highlight the topographic influence on moisture transport, *Quat. Int.*, 565, 22–30,  
647 <https://doi.org/10.1016/j.quaint.2020.09.052>, 2020.
- 648 Adhikari, N., Gao, J., Yao, T., Yang, Y., Dai, D.: The main controls of the precipitation stable  
649 isotopes at Kathmandu, Nepal, *Tellus, Ser. B Chem. Phys. Meteorol.*, 72, 1–17.

650 <https://doi.org/10.1080/16000889.2020.1721967>, 2020

651 Bohlinger, P., Sorteberg, A., Sodemann, H.: Synoptic conditions and moisture sources actuating  
652 extreme precipitation in Nepal, *J. Geophys. Res. Atmos.*, 122, 12–653,  
653 <https://doi.org/10.1002/2017JD027543>, 2017.

654 Boschi, R., Lucarini, V.: Water pathways for the Hindu-Kush-Himalaya and an analysis of three  
655 flood events, *Atmosphere*, 10, 489, <https://doi.org/10.3390/atmos10090489>, 2019.

656 Brand, W.A., Geilmann, H., Crosson, E.R., Rella, C.W.: Cavity ring-down spectroscopy versus  
657 high-temperature conversion isotope ratio mass spectrometry; a case study on delta (2) H  
658 and delta (18) O of pure water samples and alcohol/water mixtures, *Rapid Commun. mass*  
659 *Spectrom*, RCM 23, 1879–1884, <https://doi.org/10.1002/rcm.4083>, 2009.

660 Breitenbach, S.F.M., Adkins, J.F., Meyer, H., Marwan, N., Kumar, K.K., Haug, G.H.: Strong  
661 influence of water vapor source dynamics on stable isotopes in precipitation observed in  
662 Southern Meghalaya, NE India, *Earth Planet. Sci. Lett.*, 292, 212–220,  
663 <https://doi.org/10.1016/j.epsl.2010.01.038>, 2010.

664 Cai, Z., Tian, L.: Atmospheric controls on seasonal and interannual variations in the  
665 precipitation isotope in the East Asian Monsoon region, *J. Clim.*, 29, 1339–1352.  
666 <https://doi.org/10.1175/JCLI-D-15-0363.1>, 2016.

667 Cai, Z., Tian, L., Bowen, G.J.: Spatial-seasonal patterns reveal large-scale atmospheric controls  
668 on Asian Monsoon precipitation water isotope ratios, *Earth Planet. Sci. Lett.*, 503, 158–169.  
669 <https://doi.org/10.1016/j.epsl.2018.09.028>, 2018.

670 Chakraborty, S., Sinha, N., Chattopadhyay, R., Sengupta, S., Mohan, P.M., Datye, A.:



671 Atmospheric controls on the precipitation isotopes over the Andaman Islands, Bay of  
672 Bengal, *Sci. Rep.*, 6, 1–11, <https://doi.org/10.1038/srep19555>, 2016.

673 Chan, K.T.F., Chan, J.C.L., Zhang, K., Wu, Y.: Uncertainties in tropical cyclone landfall decay,  
674 *npj Clim. Atmos. Sci.*, 5, 93, <https://doi.org/10.1038/s41612-022-00320-z>, 2022.

675 Chen, F., Huang, C., Lao, Q., Zhang, S., Chen, C., Zhou, X., Lu, X., Zhu, Q.: Typhoon Control  
676 of Precipitation Dual Isotopes in Southern China and Its Palaeoenvironmental Implications,  
677 *J. Geophys. Res. Atmos.*, 126, 1–15, <https://doi.org/10.1029/2020JD034336>, 2021.

678 Chhetri, T.B., Yao, T., Yu, W., Ding, L., Joswiak, D., Tian, L., Devkota, L.P., Qu, D.: Stable  
679 isotopic compositions of precipitation events from Kathmandu, southern slope of the  
680 Himalayas, *Chinese Sci. Bull.*, 59, 4838–4846, <https://doi.org/10.1007/s11434-014-0547-4>,  
681 2014.

682 Conroy, J.L., Noone, D., Cobb, K.M., Moerman, J.W., Konecky, B.L.: Paired stable  
683 isotopologues in precipitation and vapor: A case study of the amount effect within western  
684 tropical Pacific storms, *J. Geophys. Res. Atmos.*, 121, 3290–3303,  
685 <https://doi.org/10.1002/2015JD023844>, 2016.

686 Dansgaard, W.: Stable isotopes in precipitation, *Tellus* 16, 436–468,  
687 <https://doi.org/10.3402/tellusa.v16i4.8993>, 1964

688 Delattre, H., Vallet-Coulomb, C., Sonzogni, C.: Deuterium excess in the atmospheric water  
689 vapour of a Mediterranean coastal wetland: Regional vs. local signatures, *Atmos. Chem.*  
690 *Phys.*, 15, 10167–10181, <https://doi.org/10.5194/acp-15-10167-2015>, 2015

691 Draxler, R.R., Hess, G.D.: Description of the HYSPLIT4 modeling system, 1997.

692 Fudeyasu, H., Ichiyanagi, K., Sugimoto, A., Yoshimura, K., Ueta, A., Yamanaka, M.D., Ozawa,  
693 K.: Isotope ratios of precipitation and water vapor observed in Typhoon Shanshan, J.  
694 Geophys. Res. Atmos, <https://doi.org/10.1029/2007JD009313>, 113, 2008.

695 Galewsky, J., Samuels-Crow, K.: Summertime moisture transport to the southern South  
696 American Altiplano: Constraints from in situ measurements of water vapor isotopic  
697 composition, *J. Clim.*, 28, 2635–2649, <https://doi.org/10.1175/JCLI-D-14-00511.1>, 2015.

698 Galewsky, J., Steen-larsen, H.C., Field, R.D., Risi, W.C., Schneider, M.: Stable isotopes in  
699 atmospheric water vapor and application to the hydrologic cycle., *Rev. Geophys.*  
700 submitted, 1–169, <https://doi.org/10.1002/2015RG000512>, 2016.

701 Gaona, M.F.R., Villarini, G., Zhang, W., Vecchi, G.A.: The added value of IMERG in  
702 characterizing rainfall in tropical cyclones, *Atmos. Res.*,  
703 [doi:10.1016/j.atmosres.2018.03.008](https://doi.org/10.1016/j.atmosres.2018.03.008), 209, 95–102, 2018.

704 Gedzelman, S., Lawrence, J., Gamache, J., Black, M., Hindman, E., Black, R., Dunion, J.,  
705 Willoughby, H., Zhang, X.: Probing hurricanes with stable isotopes of rain and water vapor,  
706 *Mon. Weather Rev*, [https://doi.org/10.1175/1520-0493\(2003\)131<1112:phwsio>2.0.co;2](https://doi.org/10.1175/1520-0493(2003)131<1112:phwsio>2.0.co;2),  
707 131, 1112–1127, 2003.

708 Han, X., Lang, Y., Wang, T., Liu, C.Q., Li, F., Wang, F., Guo, Q., Li, S., Liu, M., Wang, Y., Xu,  
709 A.: Temporal and spatial variations in stable isotopic compositions of precipitation during  
710 the typhoon Lekima (2019), China. *Sci. Total Environ.*, 762,  
711 <https://doi.org/10.1016/j.scitotenv.2020.143143>, 2021

712 Hassenruck-Gudipati, H.J., Andermann, C., Dee, S., Brunello, C.F., Baidya, K.P., Sachse, D.,

713 Meyer, H., Hovius, N.: Moisture Sources and Pathways Determine Stable Isotope Signature  
714 of Himalayan Waters in Nepal, *AGU Adv.*, 4, 1–19, <https://doi.org/10.1029/2022av000735>,  
715 2023.

716 He, S., Richards, K.: Stable isotopes in monsoon precipitation and water vapour in Nagqu, Tibet,  
717 and their implications for monsoon moisture, *J. Hydrol.*, 540, 615–622,  
718 <https://doi.org/10.1016/j.jhydrol.2016.06.046>, 2016.

719 Hersbach, H., Bell, B., Berrisford, P., Hirahara, S., Horányi, A., Muñoz-Sabater, J., Nicolas, J.,  
720 Peubey, C., Radu, R., Schepers, D.: The ERA5 global reanalysis, *Q. J. R. Meteorol. Soc.*  
721 146, 1999–2049, <https://doi.org/10.1002/qj.3803>, 2020

722 Hoffmann, G., Cuntz, M., Jouzel, J., Werner, M.: A systematic comparison between the  
723 IAEA/GNIP isotope network and the ECHAM 4 atmospheric general circulation model,  
724 *Isot. Water Cycle Past, Present Futur. a Dev. Sci.*, 303–320, 2005.

725 Huffman, G.J., Bolvin, D., Braithwaite, D., Hsu, K., Joyce, R., Kidd, C., Nelkin, E.J., Sorooshian,  
726 S., Tan, J., Xie, P.: Algorithm Theoretical Basis Document (ATBD) of Integrated Multi-  
727 satellitE Retrievals for GPM (IMERG), version 4.6. Nasa 29, 2017.

728 Hussain, S., Xianfang, S., Hussain, I., Jianrong, L., Dong Mei, H., Li Hu, Y., Huang, W.:  
729 Controlling Factors of the Stable Isotope Composition in the Precipitation of Islamabad,  
730 Pakistan, *Adv. Meteorol.*, 2015, 1-11, <https://doi.org/10.1155/2015/817513>, 2015.

731 Jackisch, D., Yeo, B.X., Switzer, A.D., He, S., Cantarero, D.L.M., Siringan, F.P., Goodkin, N.F.:  
732 Precipitation stable isotopic signatures of tropical cyclones in Metropolitan Manila,  
733 Philippines, show significant negative isotopic excursions, *Nat. Hazards Earth Syst. Sci.*, 22,

734 213–226, <https://doi.org/10.5194/nhess-22-213-2022>, 2022.

735 Joseph, S., Freeland, H.J.: Salinity variability in the Arabian Sea, *Geophys. Res. Lett.*, 32,  
736 <https://doi.org/10.1029/2005GL022972>, 2005.

737 Kendall, C., Caldwell, E.A.: Fundamentals of Isotope Geochemistry, *Isot. Tracers Catchment*  
738 *Hydrol.*, 51–86, <https://doi.org/10.1016/B978-0-444-81546-0.50009-4>, 1998.

739 Kleist, D.T., Parrish, D.F., Derber, J.C., Treadon, R., Wu, W.-S., Lord, S.: Introduction of the  
740 GSI into the NCEP global data assimilation system, *Weather Forecast.*, 24, 1691–1705,  
741 <https://doi.org/10.1175/2009waf2222201.1>, 2009.

742 Knapp, K.R., Kruk, M.C., Levinson, D.H., Diamond, H.J., Neumann, C.J.: The international best  
743 track archive for climate stewardship (IBTrACS) unifying tropical cyclone data, *Bull. Am.*  
744 *Meteorol. Soc.*, 91, 363–376, <https://doi.org/10.1175/2009bams2755.1>, 2010.

745 Krishnamurthy, V., Shukla, J.: Intraseasonal and seasonally persisting patterns of Indian  
746 monsoon rainfall, *J. Clim.*, 20, 3–20, <https://doi.org/10.1175/jcli3981.1>, 2007.

747 Kurita, N.: Water isotopic variability in response to mesoscale convective system over the  
748 tropical ocean, *J. Geophys. Res. Atmos.*, 118, 10,376-10,390,  
749 <https://doi.org/10.1002/jgrd.50754>, 2013.

750 Kurita, N., Noone, D., Risi, C., Schmidt, G.A., Yamada, H., Yoneyama, K.: Intraseasonal  
751 isotopic variation associated with the Madden-Julian Oscillation, *J. Geophys. Res. Atmos.*,  
752 116, 1–20, <https://doi.org/10.1029/2010JD015209>, 2011.

753 Lawrence, J.R., Gedzelman, S.D., Dexheimer, D., Cho, H.K., Carrie, G.D., Gasparini, R.,

754 Anderson, C.R., Bowman, K.P., Biggerstaff, M.I.: Stable isotopic composition of water  
755 vapor in the tropics, *J. Geophys. Res. Atmos.*, 109 (D6),  
756 <https://doi.org/10.1029/2003jd004046>, 2004.

757 Lawrence, J.R., Gedzelman, S.D., Gamache, J., Black, M.: Stable isotope ratios: hurricane Olivia,  
758 *J. Atmos. Chem.*, 41, 67–82, 2002.

759 Lawrence, J.R., Gedzelman, S.D., Zhang, X., Arnold, R.: Stable isotope ratios of rain and vapor  
760 in 1995 hurricanes, *J. Geophys. Res. Atmos.*, 103, 11381–11400,  
761 <https://doi.org/10.1029/97jd03627>, 1998.

762 Lawrence, R.J., Gedzelman, D.S.: Low stable isotope ratios of tropical cyclone rains, *Geophys.*  
763 *Res. Lett.*, 23, 527–530, <https://doi.org/10.1029/96gl00425>, 1996.

764 Lekshmy, P.R., Midhun, M., Ramesh, R.: Role of moisture transport from Western Pacific  
765 region on water vapor isotopes over the Bay of Bengal, *Atmos. Res.*, 265, 105895,  
766 <https://doi.org/10.1016/j.atmosres.2021.105895>, 2022.

767 Lekshmy, P.R., Midhun, M., Ramesh, R.: Spatial variation of amount effect over peninsular  
768 India and Sri Lanka: Role of seasonality, *Geophys. Res. Lett.*, 42(13), 5500–5507,  
769 <https://doi.org/10.1002/2015GL064517>, 2015.

770 Lekshmy, P.R., Midhun, M., Ramesh, R., Jani, R.A.:  $^{18}\text{O}$  depletion in monsoon rain relates to  
771 large scale organized convection rather than the amount of rainfall, *Sci. Rep.*, 4, 1–5.  
772 <https://doi.org/10.1038/srep05661>, 2014.

773 Li, L., Chakraborty, P.: Slower decay of landfalling hurricanes in a warming world, *Nature* 587,  
774 230–234, <https://doi.org/10.1038/s41586-020-2867-7>, 2020.

775 Li, Z., Yu, W., Li, T., Murty, V.S.N., Tangang, F.: Bimodal character of cyclone climatology in  
776 the Bay of Bengal modulated by monsoon seasonal cycle, *J. Clim.*, 26 (3), 1033–1046,  
777 <https://doi.org/10.1175/jcli-d-11-00627.1>, 2013.

778 Liebmann, B., Smith, C.A.: Description of a complete (interpolated) outgoing longwave  
779 radiation dataset, *Bull. Am. Meteorol. Soc.*, 77, 1275–1277, 1996.

780 Liu, Z., Tian, L., Yao, T., Yu, W.: Seasonal deuterium excess in Nagqu precipitation: Influence  
781 of moisture transport and recycling in the middle of Tibetan Plateau, *Environ. Geol.*, 55,  
782 1501–1506, <https://doi.org/10.1007/s00254-007-1100-4>, 2008.

783 Midhun, M., Lekshmy, P.R., Ramesh, R.: Hydrogen and oxygen isotopic compositions of water  
784 vapor over the Bay of Bengal during monsoon, *Geophys. Res. Lett.*, 40, 6324–6328,  
785 <https://doi.org/10.1002/2013GL058181>, 2013.

786 Midhun, M., Pr, L., Ramesh, R., Yoshimura, K., Kk, S.: The effect of monsoon circulation on the  
787 stable isotopic composition of rainfall, *J. Geophys. Res. Atmos.*, 123, 5205–5221,  
788 <https://doi.org/10.1029/2017JD027427>, 2018.

789 Mohapatra, M., Srivastava, A.K., Balachandran, S., Geetha, B.: Inter-annual variation and trends  
790 in Tropical Cyclones and Monsoon Depressions over the North Indian Ocean. Observed  
791 Climate Variability and Change over the Indian Region, *Springer Geology*, 89–106,  
792 [https://doi.org/10.1007/978-981-10-2531-0\\_6](https://doi.org/10.1007/978-981-10-2531-0_6), 2016.

793 Munksgaard, N.C., Zwart, C., Kurita, N., Bass, A., Nott, J., Bird, M.I.: Stable isotope anatomy of  
794 tropical cyclone ita, North-Eastern Australia, April 2014, *PLoS One* 10, 1–15,  
795 <https://doi.org/10.1371/journal.pone.0119728>, 2015.

796 Noone, D.: Pairing measurements of the water vapor isotope ratio with humidity to deduce  
797 atmospheric moistening and dehydration in the tropical midtroposphere, *J. Clim.*, 25, 4476–  
798 4494, <https://doi.org/10.1175/JCLI-D-11-00582.1>, 2012.

799 Pandya, U., Khandelval, S., Sanghvi, H., Joshi, E., Vekaria, G.L., Jaaffrey, S.N.A., Soni, M.:  
800 Cyclone ‘TAUKTAE’-Observed through data & satellite images, 2021.

801 Paul, S., Chowdhury, S.: Investigation of the character and impact of tropical cyclone Yaas: a  
802 study over coastal districts of West Bengal, India, *Saf. Extrem. Environ.*, 3, 219–235,  
803 <https://doi.org/10.1007/s42797-021-00044-y>, 2021.

804 Payne, V.H., Noone, D., Dudhia, A., Piccolo, C., Grainger, R.G.: Global satellite measurements  
805 of HDO and implications for understanding the transport of water vapour into the  
806 stratosphere, *Q. J. R. Meteorol. Soc.*, 133, 1459–1471, <https://doi.org/10.1002/qj>, 2007.

807 Pfahl, S., Sodemann, H.: What controls deuterium excess in global precipitation? *Clim. Past*, 10,  
808 771–781, <https://doi.org/10.5194/cp-10-771-2014>, 2014..

809 Rahul, P., Ghosh, P., Bhattacharya, S.K., Yoshimura, K.: Controlling factors of rainwater and  
810 water vapor isotopes at Bangalore, India: Constraints from observations in 2013 Indian  
811 monsoon, *J. Geophys. Res.*, 121, 13,936-13,952, <https://doi.org/10.1002/2016JD025352>,  
812 2016.

813 Rajeev, A., Mishra, V.: Observational evidence of increasing compound tropical cyclone-moist  
814 heat extremes in India, *Earth’s Futur.*, 10, e2022EF002992,  
815 <https://doi.org/10.1029/2022ef002992>, 2022.

816 Risi, C., Bony, S., Vimeux, F.: Influence of convective processes on the isotopic composition

817 ( $\delta^{18}\text{O}$  and  $\delta\text{D}$ ) of precipitation and water vapor in the tropics: 2. Physical interpretation of  
818 the amount effect, *J. Geophys. Res. Atmos.*, 113, 1–12,  
819 <https://doi.org/10.1029/2008JD009943>, 2008.

820 Sánchez-Murillo, R., Durán-Quesada, A.M., Esquivel-Hernández, G., Rojas-Cantillano, D.,  
821 Birkel, C., Welsh, K., Sánchez-Llull, M., Alonso-Hernández, C.M., Tetzlaff, D., Soulsby,  
822 C., Boll, J., Kurita, N., Cobb, K.M.: Deciphering key processes controlling rainfall isotopic  
823 variability during extreme tropical cyclones, *Nat. Commun.*, 10, 1–10,  
824 <https://doi.org/10.1038/s41467-019-12062-3>, 2019.

825 Saranya, P., Krishan, G., Rao, M.S., Kumar, S., Kumar, B.: Controls on water vapor isotopes  
826 over Roorkee, India: Impact of convective activities and depression systems, *J. Hydrol.*, 557,  
827 679–687, <https://doi.org/10.1016/j.jhydrol.2017.12.061>, 2017.

828 Singh, A., Jani, R.A., Ramesh, R.: Spatiotemporal variations of the  $\delta^{18}\text{O}$ –salinity relation in the  
829 northern Indian Ocean, *Deep Sea Res., Part I* 57 (11), 1422–1431,  
830 <https://doi.org/10.1016/j.dsr.2010.08.002>, 2010.

831 Steen-Larsen, H.C., Sveinbjörnsdóttir, A.E., Peters, A.J., Masson-Delmotte, V., Guishard, M.P.,  
832 Hsiao, G., Jouzel, J., Noone, D., Warren, J.K., White, J.W.C.: Climatic controls on water  
833 vapor deuterium excess in the marine boundary layer of the North Atlantic based on 500  
834 days of in situ, continuous measurements, *Atmos. Chem. Phys.*, 14, 7741–7756,  
835 <https://doi.org/10.5194/acp-14-7741-2014>, 2014.

836 Sun, C., Tian, L., Shanahan, T.M., Partin, J.W., Gao, Y., Piatrunia, N., Banner, J.: Isotopic  
837 variability in tropical cyclone precipitation is controlled by Rayleigh distillation and cloud  
838 microphysics, *Commun. Earth Environ.*, 3, <https://doi.org/10.1038/s43247-022-00381-1>,



839 2022.

840 Tian, L., Masson-Delmotte, V., Stievenard, M., Yao, T., Jouzel, J.: Tibetan Plateau summer  
841 monsoon northward extent revealed by measurements of water stable isotopes, *J. Geophys.*  
842 *Res.*, 106, 28081–28088, <https://doi.org/10.1029/2001JD900186>, 2001.

843 Tian, L., Yu, W., Schuster, P.F., Wen, R., Cai, Z., Wang, D., Shao, L., Cui, J., Guo, X.: Control  
844 of seasonal water vapor isotope variations at Lhasa, southern Tibetan Plateau, *J. Hydrol.*,  
845 580, 124237, <https://doi.org/10.1016/j.jhydrol.2019.124237>, 2020.

846 Tian, L., Yao, T., Numaguti, A., Sun, W.: Stable isotope variations in monsoon precipitation on  
847 the Tibetan Plateau, *J. Meteorol. Soc. Japan.*, 79, 959–966,  
848 <https://doi.org/10.2151/jmsj.79.959>, 2001.

849 Uemura, R., Matsui, Y., Yoshimura, K., Motoyama, H., Yoshida, N.: Evidence of deuterium  
850 excess in water vapor as an indicator of ocean surface conditions, *J. Geophys. Res. Atmos.*,  
851 113, <https://doi.org/10.1029/2008jd010209>, 2008.

852 Verma, K., Gupta, A., 2021. Cyclone Tauktae: Cyclones, Their Impacts and Disasters Risk  
853 Management.

854 Villarini, G., Smith, J.A., Baeck, M.L., Marchok, T., Vecchi, G.A.: Characterization of rainfall  
855 distribution and flooding associated with US landfalling tropical cyclones: Analyses of  
856 Hurricanes Frances, Ivan, and Jeanne (2004), *J. Geophys. Res. Atmos.*, 116, [https://doi.org](https://doi.org/10.1029/2011jd016175)  
857 [/10.1029/2011jd016175](https://doi.org/10.1029/2011jd016175), 2011.

858 Wei, Z., Yoshimura, K., Okazaki, A., Ono, K., Kim, W., Yokoi, M., Lai, C.T.: Understanding  
859 the variability of water isotopologues in near-surface atmospheric moisture over a humid

860 subtropical rice paddy in Tsukuba, Japan, *J. Hydrol.*, 533, 91–102,  
861 <https://doi.org/10.1016/j.jhydrol.2015.11.044>, 2016.

862 Worden, J., Noone, D., Bowman, K.: Importance of rain evaporation and continental convection  
863 in the tropical water cycle, *Nature*, 445, 528–532, <https://doi.org/10.1038/nature05508>,  
864 2007.

865 Xu, T., Sun, X., Hong, H., Wang, X., Cui, M., Lei, G., Gao, L., Liu, J., Lone, M.A., Jiang, X.:  
866 Stable isotope ratios of typhoon rains in Fuzhou, Southeast China, during 2013–2017, *J.*  
867 *Hydrol.*, 570, 445–453, <https://doi.org/10.1016/j.jhydrol.2019.01.017>, 2019.

868 Yoshimura, K.: Stable Water Isotopes in Climatology, Meteorology, and Hydrology: A Review,  
869 *J. Meteorol. Soc. Japan*, 93, 513–533, <https://doi.org/10.2151/jmsj.2015-036>, 2015.

870 Yu, W., Yao, T., Tian, L., Ma, Y., Ichiyanagi, K., Wang, Y., Sun, W.: Relationships  
871 between  $\delta^{18}\text{O}$  in precipitation and air temperature and moisture origin on a south-north  
872 transect of the Tibetan Plateau, *Atmos. Res.*, 87, 158–169,  
873 <https://doi.org/10.1016/j.atmosres.2007.08.004>, 2008.

874 Yu W, Yao T, Tian L, Ma Y, Wen R, Devkota LP, Wang W, Qu D, Chhetri TB.: Short-term  
875 variability in the dates of the Indian monsoon onset and retreat on the southern and northern  
876 slopes of the central Himalayas as determined by precipitation stable isotopes, *Clim. Dyn.*,  
877 47, 159-72, <https://doi:10.1007/s00382-015-2829-1>, 2016.

878

879